nature communications

Article

https://doi.org/10.1038/s41467-026-69118-4

An isolable phosphaalumene(3) capable of small molecule activation via unique modes of reactivity

Received: 27 July 2025

Accepted: 22 January 2026

Published online: 05 February 2026

Check for updates

Yan Cha[1,2], Zhaoziyuan Yang[1,2], Xiao Zhuang[1], Pengyu Gao[1], Tingting Liu[1], Fei Luo[1], Xianjia Ni[1], Qing Luo[1] & Wei Lu[1]

The chemistry of phosphaalumenes [R–Al=P–R'] featuring multiple bonds between phosphorus and aluminum remains largely unexplored. Here we show the syntheses of a phosphaalumene(3) through either the reaction of ^{Dipp}NacNacM (^{Dipp}NacNac = HC[(CMe)N(2,6-^{i}Pr$_2$C$_6$H$_3$)]$_2$, M = Al) with a bisphosphirane-fused anthracene (**1**) or with a phospha-Wittig reagent (**2**) under mild conditions. This phosphaalumene exhibits reactivities that stand in contrast to those of previously reported transient species **II**, especially in its ability to activate small molecules such as dihydrogen (H_2), white phosphorus (P_4), isocyanides, CO_2, N_2O, trimethylsilyl azide ($TMSN_3$), diphenyl diselenide (PhSeSePh), $PhSiH_3$, $PhNH_2$, styrene and 1-ethynyl-4-methylbenzene. It has been found in this research that the ligand environment can have a subtle but profound impact on the reactivity of phosphaalumenes.

The construction of heterodiatomic multiple bonds between group 13 and 15 elements is a fascinating area of research because of the unusual bonding properties and reactivities of these compounds, not found with their carbon analogues[1–6]. The polarities of such bonds, arising from the electronegativity differences between E_{13} and E_{15} elements, render these species highly reactive and potentially useful in the activation of small molecules and inert bonds. While much of this chemistry was pioneered with kinetically and electronically stabilized iminoboranes (R–B$^-$≡N$^+$–R)[7–9], examples of compounds bearing B = E_{15} (E_{15} = P[10–22], As[23,24]) bonds or E_{13} = N (E_{13} = Al[25–31], Ga[25,32,33], In[32,34]) bonds, systems in which one element has a principal quantum number (n) greater than 2, have also been well described. The construction of heavier E_{13} = E_{15} multiple bonds (E_{13} = Al, Ga, In; E_{15} = P, As, Sb)[35–38] is hindered by a number of complicating factors, including the inherent weaknesses of these π-bonds stemming from inefficient overlap of the p_π-p_π orbitals on descending the group, their strong tendency to undergo oligomerization, and the lack of reliable synthetic protocols and appropriate precursors.

A landmark discovery by Power and coworkers demonstrated that M = N (M = Al, Ga) multiple bonds can be directly accessed by employing group 13 carbenoids ^{Dipp}NacNacM (M = Al, Ga) and organoazides[25]. This was then followed by the synthesis of a range of phosphagallenes containing P = Ga double bonds[39–47]. By contrast, compounds with Al = P double bonds remain exceedingly rare, presumably due to their increased polarities and thus significantly enhanced reactivities compared to Ga = P double bonds[48,49]. A major breakthrough was reported by Hering-Junghans and Braunschweig in 2021, describing the synthesis of the first isolable phosphaalumene **I**, which was characterized by a six-coordinate Al center and a two-coordinate P center (Fig. 1a)[50]. The same groups went on to detail how the pronounced π(Al = P)-character of these species enabled the activation of C–C and B–N multiple bonds, as well as organoazides[51–53]. It was demonstrated that when **1** reacts with unsaturated C–C bonds, it forms a multitude of unique P, Al-heterocycles that cannot be directly produced by other means. Furthermore, the reaction between **1** and organoazides revealed reaction patterns that significantly differed from those documented for alkyne and 1,3-dipolar molecules, thereby offering new perspectives on chemical reactions. Despite these advances, the synthesis of low-coordinate Al = P bonds remains a formidable challenge. Pioneering studies from the groups of Hering-Junghans, Braunschweig, and Goicoechea aimed at developing phosphaalumene(3) species by integrating a two-coordinate Al(I) species,

[1]Key Laboratory of Green Chemistry & Technology of Ministry of Education, College of Chemistry Sichuan University, Chengdu, P. R. China. [2]These authors contributed equally: Yan Cha, Zhaoziyuan Yang. e-mail: wei.lu@scu.edu.cn

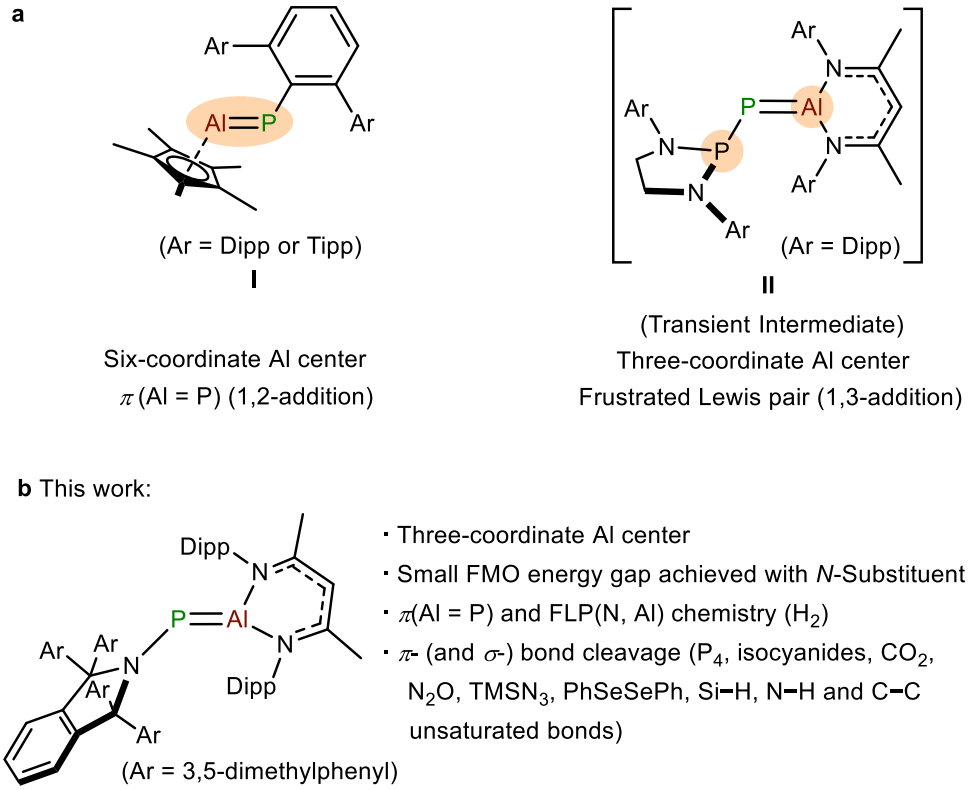

Fig. 1 | Reported phosphaalumenes and this work. a Reported examples of phosphaalumenes (**I-II**). **b** This work: substituent and coordination number effects on the chemical behavior of an isolable phosphaalumene(3) [Dipp = 2,6-^{i}Pr$_2$C$_6$H$_3$, Tipp = 2,4,6-^{i}Pr$_3$C$_6$H$_2$].

^{Dipp}NacNacM (M = Al), with mono-coordinate phosphinidene surrogates. However, this endeavor succeeded only in yielding fleeting species that could not be isolated under ambient conditions[48,49]. Among these transient compounds, phosphanyl phosphaalumene (**II**) was found to be highly reactive in the activation of kinetically challenging substrates such as H_2 via an FLP-type pathway through the cooperative action of the Al and the pendant P centers and could be captured as a Lewis base (tetrahydrofuran) adduct[49]. Inspired by the advantageous characteristics of these transient phosphaalumenes in bond activation, we sought to develop an isolable phosphaalumene(3) and explore its reactivity patterns with small molecules.

Preliminary theoretical studies suggested that the incorporation of a nitrogen atom bonded to the phosphorus in an Al = P complex, in contrast to other elements like B, C, O, and P, significantly narrows the energy gap between the frontier molecular orbitals (FMO) associated with P = Al double bonds (Fig. S163). This characteristic is a determining factor in promoting the activation of kinetically challenging substrates such as H_2. As such, we sought to develop novel phosphaalumenes, kinetically stabilized by sterically bulky *N*-substituents. Herein, we report the synthesis of a phosphaalumene(3) supported by a NacNac ligand and an isoindoline moiety. Remarkably, this species shows both π(Al = P)-behavior and FLP-type character in reactions with H_2. We also demonstrate how Al = P π- (and σ-) bond cleavage is instrumental in their reactions with P_4, isocyanides, CO_2, N_2O, $TMSN_3$, PhSeSePh, E-H bonds (E = Si, N), styrene, and 1-ethynyl-4-methylbenzene.

Results

Synthesis and characterization of 3

We have recently reported the synthesis of a bisphosphrane-fused anthracene **1** that functioned as a highly effective phosphinidene surrogate in small molecule activation[54,55]. This compound features a π-donating isoindoline group and a sterically congested phosphorus center, which prompted us to investigate its reaction with Al(I) as a route to Al = P double bonds. The reaction of **1** with two equivalents of ^{Dipp}NacNacM (M = Al) in benzene at 50 °C led to the formation of a reddish-brown solution of **3** (Fig. 2a). The ^{31}P NMR spectrum of the crude reaction mixture indicated the presence of several phosphorus-containing species, which after recrystallization gave **3** as dark-red crystals in 13% yield. Alternatively, when a benzene solution of **1** and two equivalents of ^{Dipp}NacNacM was subjected to UV light irradiation at 365 nm, compound **3** was obtained in 18% yield. Despite the successful synthesis and characterization, the purification of **3** remained a challenge, primarily due to the quantitative formation of anthracene during the fragmentation of **1**. To our delight, when the phospha-Wittig reagent **2** was employed as a phosphinidene precursor it reacted stoichiometrically with ^{Dipp}NacNacM in benzene at ambient temperature to yield **3**, which was isolated as a red-brown powder in 91% yield. The ^{31}P NMR spectrum of **3** showed a sharp resonance at 9.0 ppm, which is downfield-shifted compared to those observed in **1** and **2** (−99.8 and −14.8 ppm, respectively), and also to those of **I** (Ar = Dipp: −203.9 ppm and Ar = Tipp: −208.9 ppm) (Table S3). Single crystals of **3** were obtained from a saturated *n*-hexane solution in a glove box. Single-crystal X-ray diffraction analysis (SC-XRD) revealed a two-coordinate P center and a three-coordinate Al center (Fig. 2b). The length of Al–P bond (2.2340(8) Å) is close to those reported by Hering-Junghans and Braunschweig (2.2113(6) and 2.2022(6) Å) (Table S3)[49,50]. Both the Al3 and N1 centers are trigonal-planar with sums of bond angles measuring 357.2° (Al3) and 355.0° (N1), respectively.

The electronic features of **3** were further examined by DFT calculations at the PBE0-D3 (BJ)/Def2-SVP level of theory. As shown in Fig. 2c. the highest occupied molecular orbital (HOMO) of **3** is dominated by the Al–P π-bonding orbital, while the HOMO − 1 is comprised of the Al–P σ-bonding orbital with some contribution from the lone pairs of N1 and P2. The HOMO − 2 predominantly reflects the π-bonding interactions along the N1–P2 bond and in the aryl substituents

https://doi.org/10.1038/s41467-026-69118-4

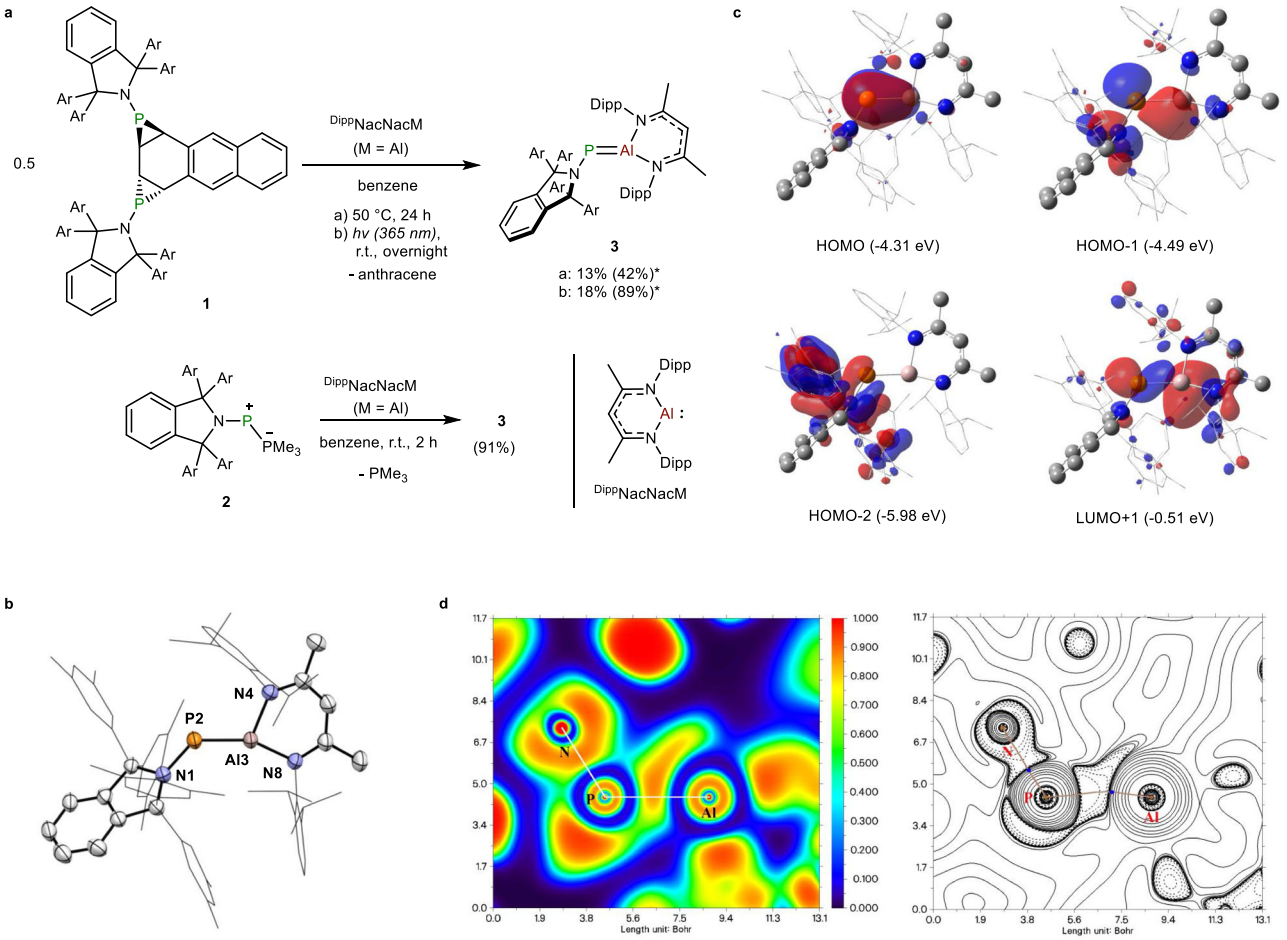

Fig. 2 | Syntheses, Solid-state structure and theoretical studies of 3. a Syntheses of **3** from bisphosphrane-fused anthracene **1** or phospha-Wittig reagent **2** with ^{Dipp}NacNacM (M = Al, Ar = 3,5-dimethylphenyl, *indicates NMR yield). **b** Solid-state structure of **3** (Hydrogen atoms and solvent molecules are omitted for clarity; Thermal ellipsoids are set at the 50% probability level). **c** Selected frontier molecular orbitals of **3** (DFT calculations were performed at the PBE0-D3(BJ)/Def2-SVP level of theory). **d** Depiction of the ELF (left) and contour-line plot of the Laplacian of the electron density (right) of **3** in the NPAl-plane[56].

attached to the isoindoline moiety. Remarkably, the lowest unoccupied molecular orbital (LUMO) of **3** (Fig. S164) is localized on the *β*-diketiminate ligand backbone due to the contribution of its low-lying π^* orbital. The LUMO + 1 mainly corresponds to the P–Al σ^* orbital, which resembles closely the LUMO of **I**. Natural bond orbital (NBO) analysis calculated at the PBE0-D3(BJ)/Def2-TZVP level of theory reveals the presence of one Al–P σ bonding interaction and one Al–P π bonding interaction (14.77% Al, 85.23% P), along with a Wiberg bond index (WBI) of 1.41, which further corroborates the Al = P double bond character. Natural population analysis (NPA) calculates the charges on the Al3-P2 moiety to be +1.43 for Al3 and −0.29 for P2, indicative of a polarized π-bonding interaction. The UV-vis spectrum of **3** in toluene displays an absorption maximum at 414 nm, which is assigned to the HOMO − 1 to LUMO + 1 transition. The simulated spectrum by a time-dependent density functional theory (TD-DFT) identifies three further maxima at 605, 553, and 468 nm, attributed to S1, S2, and S3, respectively. The latter absorptions are not clearly observed in the experiment spectrum; their low oscillator strengths (Fig. S145 and Table S7) make them too faint to resolve, and they are likely obscured by band broadening or solvent effects.

Additionally, the Electron Localization Function (ELF)[57] and the Laplacian of the electron density were analyzed in the NAlP plane to provide validation of the NBO findings. The ELF depiction in the NPAl plane of 3 (Fig. 2d, left) reveals a lone pair on the P atom with substantial *s*-character. This is complemented by the Laplacian plot (Fig. 2d, right), which shows valence shell charge concentrations (VSCCs) at the P atom and bond critical points shifted toward Al, consistent with a polarized P–Al bond. The P–Al bond displays an electron density of 0.072 e·bohr^{-3} at its bond critical point (BCP). This, along with a negative energy density (−0.028 a.u.) and a positive Laplacian of the electron density, suggests a polarized covalent bond. Furthermore, its substantial ellipticity ($\varepsilon = 0.481$) decisively indicates considerable π-character, aligning with a double bond. In comparison, the P–N BCP analysis yields $\rho(r) = 0.151$ e·bohr^{-3}, a positive $\nabla^2\rho(r)$, $H(r) = -0.117$ a.u., and $\varepsilon = 0.015$, which are indicative of pronounced single bond character.

3 can be stored in a glovebox as a solid for weeks, but slowly decomposes to give a complex mixture when heated to 50 °C in C_6D_6. The increased thermal sensitivity relative to **I** prompted us to investigate its reactivity with small molecules such as H_2, P_4, isocyanides, CO_2, N_2O, $TMSN_3$, PhSeSePh, $PhSiH_3$, $PhNH_2$, styrene, and 1-ethynyl-4-methylbenzene, allowing for the evaluation of the substituent effect in the chemical behavior of **3** in comparison with **I** and **II**.

Reactions of 3 with $H_2(D_2)$: π(Al = P) Bonding and Al/N Frustrated Lewis Pair Character

First, we examined the reactivity of **3** with H_2. Treatment of a red-brown solution of **3** in benzene with H_2 (1 Bar) at 40 °C led to the formation of an orange mixture within 12 h (Fig. 3). Interestingly, ^{31}P NMR experiments indicated the presence of two hydrogenation

https://doi.org/10.1038/s41467-026-69118-4

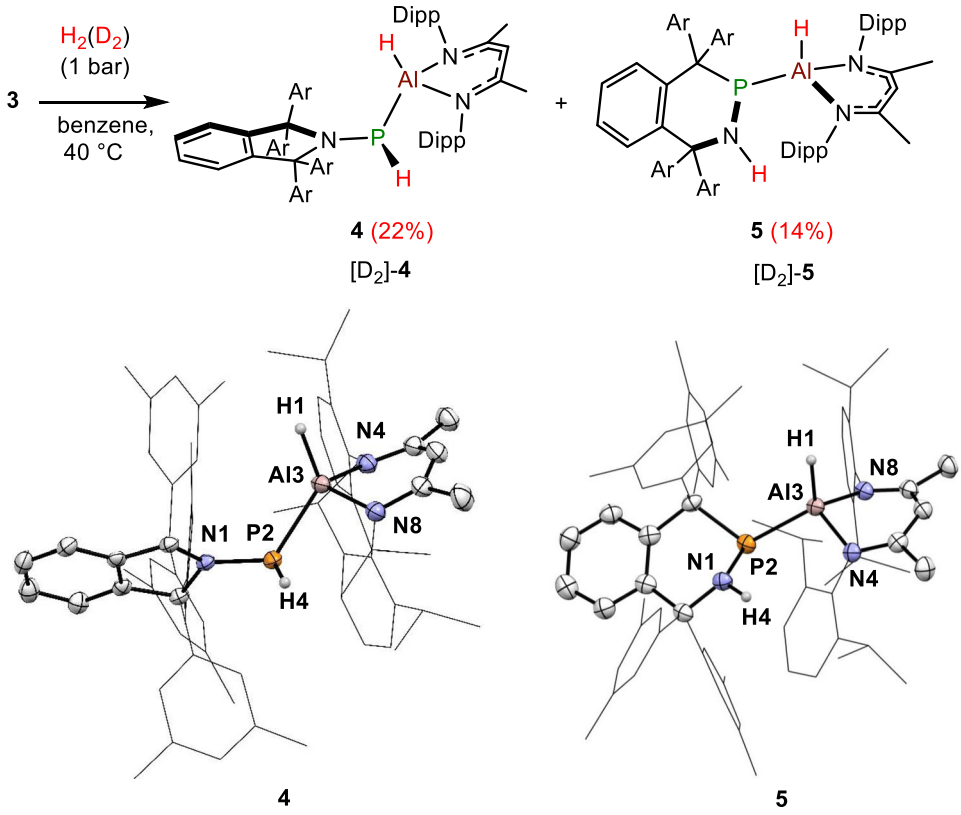

Fig. 3 | Reaction of 3 with $H_2(D_2)$. Ellipsoids of the solid-state structures of **4** (bottom, left) and **5** (bottom, right) are shown at the 50% probability level. All hydrogen atoms except those bound to P2 and Al3 of **4**, N1 and Al3 of **5** have been omitted for clarity.

products in a ratio of 1:0.54. Compounds **4** and **5** were obtained by recrystallization from a saturated *n*-hexane solution, resulting in colorless and orange crystals with yields of 22% and 14%, respectively. The ^{31}P NMR spectrum of **4** displayed a doublet of doublet at −87.8 ppm ($^1J_{P\text{-}H}$ = 204.5 Hz, $^2J_{P\text{-}H}$ = 18.6 Hz), while **5** revealed a doublet at 55.3 ppm ($^2J_{P\text{-}H}$ = 20.1 Hz), which both collapsed to singlets upon proton decoupling. In their solid-state IR spectra, **4** exhibited two vibrations characteristic of P–H and Al–H at 2244 cm^{-1} and 1834 cm^{-1}, while **5** showed two distinct vibrations for N–H and Al–H at 3347 cm^{-1} and 1817 cm^{-1}, respectively. A labelling study employing D_2 smoothly yielded a mixture of [D_2]-**4** and [D_2]-**5** (Figs. S29 and S30). The structures of **4** and **5** were unambiguously determined by SC-XRD. The solid-state structure of **4** revealed the presence of an Al–P single bond (2.3664(10) Å), with the Al atom positioned in a tetrahedral geometry and the P atom in a trigonal-pyramidal arrangement. These results were indicative of the addition of H_2 across the Al–P double bond in a 1,2 fashion. Notably, **3** also functions as seen in FLP systems in the reaction with H_2, resulting in the 1,3-addition of H_2 to the N1 and Al3 atoms, which is then followed by the integration of P2 into the NC_4 ring to yield **5**[49,58,59]. In the solid-state structure of **5**, the Al–P bond distance (2.4355(6) Å) is slightly longer than that found in **4**. It is worth highlighting that the formation of **4** represents a rare example of H_2 splitting over heavier E_{13} = E_{15} multiple bonds[28,60].

To gain insight into the various possible reaction mechanisms, the pathways for the formation of **4** and **5** were elucidated through theoretical calculations using the simplified model **3′** and H_2 at the B3LYP-D3(BJ)/Def2-TZVPPD-SMD(benzene)//PBE0-D3(BJ)/Def2-SVP level of theory. A mechanism that is consistent with these investigations is shown in Fig. 4. The addition of H_2 across the Al = P double bond of **3′** produces **4′** via **TS1′** with a total energy barrier of 24.98 kcal•mol^{-1}. In a competitive reaction to yield **5′**, the initial step involves a FLP-like H_2 activation over the Al center and the pendant isoindoline moiety of **3′**, giving **INT1** via **TS1** with a barrier of 24.47 kcal•mol^{-1}. Subsequent ring expansion of the pendant isoindoline ligand furnishes **INT2** via **TS2** with a small energy barrier of 3.19 kcal•mol^{-1}. In the next step, ring contraction of **INT2** via a 1,3-shift of the phosphorus atom gives **INT3** via **TS3** (26.63 kcal•mol^{-1}). In the last step, stereo-inversion and conformational change afford **5′**. Overall, the formation of **4′** and **5′** are thermodynamically favored by 26.59 and 25.91 kcal•mol^{-1}, respectively. The rate determining step (**INT2** to **INT3**) for the formation of **5′** (26.63 kcal•mol^{-1}) is energetically less favorable compared to that of **4′** (24.98 kcal•mol^{-1}). To ascertain the reversibility of H_2 activation, we reacted **4** and **5** with 1 atm of D_2 in benzene-d_6. Nonetheless, neither H–D exchange nor any novel products were detected (Figs. S37 and S38). To assess the hydrogen transfer ability of compounds **4** and **5**, their reactions with ketones were investigated. When a benzene-d_6 solution of these compounds was mixed with fluorenone at room temperature, the color of the solution transformed from yellow to red after two days. ^{1}H NMR and ^{31}P NMR spectroscopy confirmed that compound **4** remained unreacted, while compound **5**'s characteristic signals completely disappeared. (Figs. S39 and S40). Unfortunately, all attempts to isolate this red product were unsuccessful.

Reactions of 3 with P_4, Isocyanides, CO_2, N_2O, $TMSN_3$, and PhSeSePh: Al = P π- and σ-Bond Cleavage

The controlled activation of P_4 with main-group homoatomic double bonds such as diborenes[61–63], dialumenes[64], disilenes[65–67], dithallene[68], and distannynes[69], has been a major focus of recent interest, as it is a versatile reagent in generating organophosphorus substances. As far as we know, there is only one example of P_4 activation facilitated by a heteroatomic double bond, specifically the phosphasilenes developed by Driess, which degrade P_4 through the cleavage of the π and the σ bonds of the P = Si linkage[70]. When **3** was treated with P_4 at ambient

https://doi.org/10.1038/s41467-026-69118-4

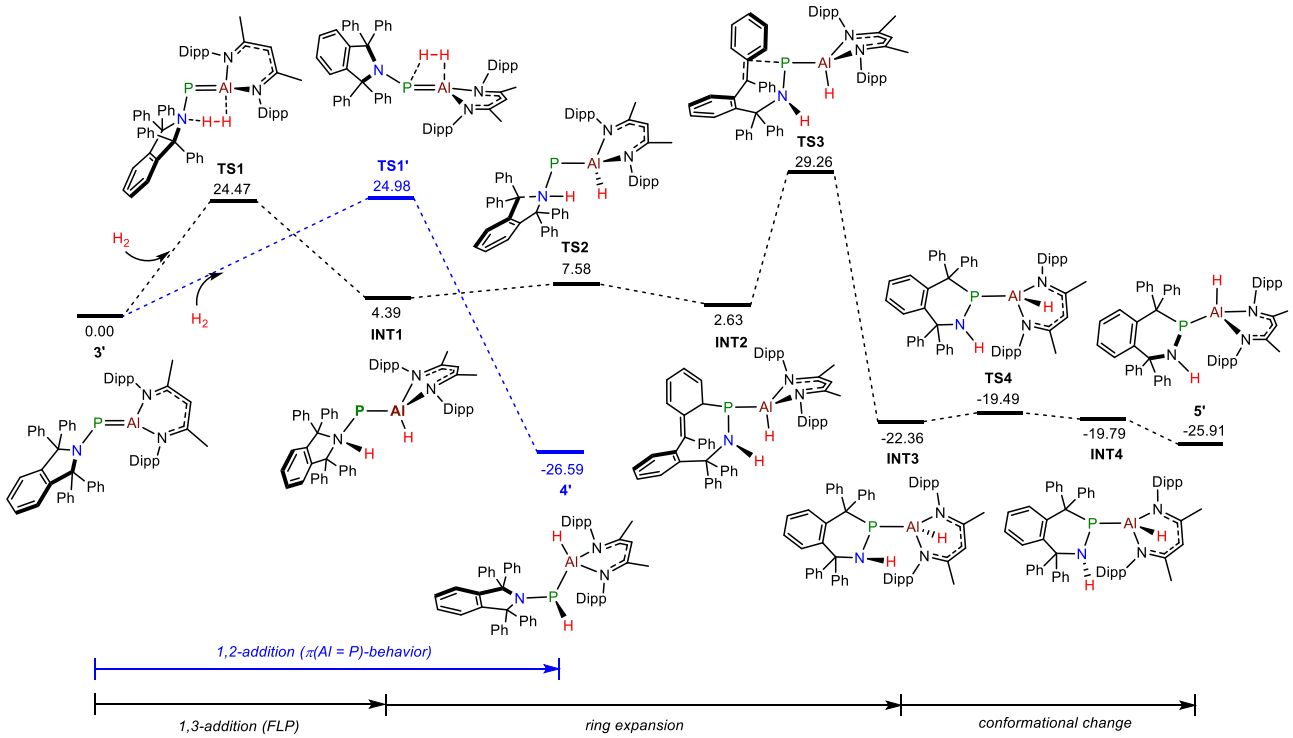

Fig. 4 | DFT-calculated free-energy profile (kcal•mol^{-1}) for the proposed mechanism of H_2 activation by 3. The free energy was obtained at the B3LYP-D3(BJ)/Def2-TZVPPD-SMD(benzene)//PBE0-D3(BJ)/Def2-SVP level of theory.

conditions, an orange mixture was formed, from which a stoichiometric amount of **6** was obtained as an orange solid (Fig. 5). The ^{31}P NMR spectrum of **6** shows five multiplet resonances at 94.5 (qd, $^{1}J_{P\text{-}P}$ = 187.9 Hz, $^{2}J_{P\text{-}P}$ = 51.8 Hz), −21.9 (dd, $^{1}J_{P\text{-}P}$ = 236.5 Hz, $^{2}J_{P\text{-}P}$ = 50.2 Hz), −81.0 (ddd, $^{1}J_{P\text{-}P}$ = 267.3 Hz, $^{2}J_{P\text{-}P}$ = 121.5 Hz, $^{3}J_{P\text{-}P}$ = 16.2 Hz), −112.8 (tt, $^{1}J_{P\text{-}P}$ = 124.8 Hz, $^{2}J_{PP}$ = 53.5 Hz), and −126.3 ppm (dddd, $^{1}J_{P\text{-}P}$ = 265.7 Hz, $^{2}J_{P\text{-}P}$ = 139.3 Hz, $^{2}J_{P\text{-}P}$ = 124.8 Hz, $^{3}J_{P\text{-}P}$ = 21.1 Hz), indicating the cleavage of P–P σ-bonds of P_4 and the formation of a non-symmetrical structure. The solid structure of **6** was determined by SC-XRD analysis, revealing a complete cleavage of the Al = P double bond to form an AlP_5 cage scaffold, tethered by an isoindoline and a NacNac ligands (Fig. 6). This reaction facilitates a two-electron oxidation of the Al = P double bond of **3**, yielding **6** characterized by P(I) and Al(III) centers, which is in line with the reactivity reported for dialumenes and disilenes[63,65]. The formation of **6** provides a noteworthy instance of P_4 activation accomplished via an $E_{13} = E_{15}$ double bond.

Isocyanides are important C1 building blocks in the context of multicomponent reactions and materials science. The reductive coupling of isocyanides has been well documented for low-valent aluminum systems such as ^{Ar}NacNacM[71], dialumane[72], and the aluminyl anion[73], but it is not known for phosphaalumenes. As such, we examined the reactivity of **3** with isocyanides, specifically ^{t}BuNC and PhNC, which resulted in the complete rupture of the Al = P bond. Upon reacting **3** with two equivalents of ^{t}BuNC, **7′** rapidly emerged, but then slowly isomerized at ambient temperature, yielding a 1:10 mixture of **7′** and **7**. This gradual transformation of **7′** into **7** impeded efforts to obtain single crystals of **7′**, thereby precluding the validation of its solid-structure (Figs. S61 and S62). Similarly, when **3** was treated with three equivalents of ^{t}BuNC, only a 1:10 mixture of **7′** and **7** resulted, with no additional products detected (Figs. S61–S64). In the ^{31}P NMR spectra, the resonances for the phosphorus atoms in **7′** and **7** appeared as singlets at 119.3 ppm and 138.9 ppm, respectively. In a separate experiment, compound **8** was isolated in 62% yield when **3** was reacted with two equivalents of PhNC, and subsequent treatment of **8** with an additional equivalent of PhNC produced **9** in almost quantitative yield (Figs. S71 and S72). Alternatively, combining **3** with three equivalents of PhNC directly afforded **9** in 45% yield. The ^{31}P NMR spectra of **8** and **9** showed signal at 46.3 and 112.0 ppm, respectively.

The structures of **7, 8**, and **9** were determined by SC-XRD. The solid-state structure of **7** revealed the incorporation of two equivalents of ^{t}BuNC into the Al = P double bond, yielding a spirocyclic structure constructed of a four-membered $AlNC_2$ ring and an AlN_2C_3 heterocycle. The aluminum atom is tetra-coordinated with the ^{Dipp}NacNac and cyclic(alkyl)(imino) ligands, while the phosphorus atom adopts a two-coordinate geometry. Compound **8** is characterized by a bicyclic core comprising two interconnected rings. The PC_2N and $AlNC_2$ rings, which are fused within **8**, exhibit a slight twist, with their internal tetragon angle sums measuring 359.2° and 356.3°, correspondingly. The solid-state structure of **9** confirmed the integration of three equivalents of PhNC into **3**, furnishing a fused bicyclic system. All five atoms of the $AlNC_3$ ring are coplanar with the sum of internal pentagon angles of 539.74°, while the fused PNC_2 ring adopts a slightly butterfly-like geometry with a P2-C3-C4-N5 torsion angle of −14.14°. Given that reactions of **7** with less sterically encumbered isocyanides may enable the synthesis of more complex heterocycles, such as aluminum phosphaguanidinates[74], we studied the reaction of **7** with an excess of PhNC, which yielded a complex mixture that precluded further purification (Figs. S81 and S82).

To investigate the reactivity of **3** with unsaturated bonds, we subjected it to treatment with CO_2. Exposure of a C_6D_6 solution of **3** to an atmosphere of CO_2 at ambient temperature led instantaneously and cleanly to the formation of **10**. The ^{31}P NMR of **10** displays a singlet at 21.8 ppm, which is downfield-shifted with respect to that of **3**. In the $^{13}C\{^{1}H\}$ NMR spectrum, the resonance for the carbonyl carbons appears as a doublet at 173.7 ppm (d, $^{1}J_{P\text{-}C}$ = 21.0 Hz), which is comparable to that of a reported phosphine-dicarboxylate compound obtained from the reaction of phosphagallene (P = Ga) with CO_2[41,44]. The solid-state structure of **10** was determined by SC-XRD, revealing the cleavage of the Al = P bond and double CO_2 addition, yielding a product featuring a boat-type six-membered PC_2O_2Al ring, which bears a resemblance to those found in reactions involving arsanyl-phosphagallene or gallyl-

https://doi.org/10.1038/s41467-026-69118-4

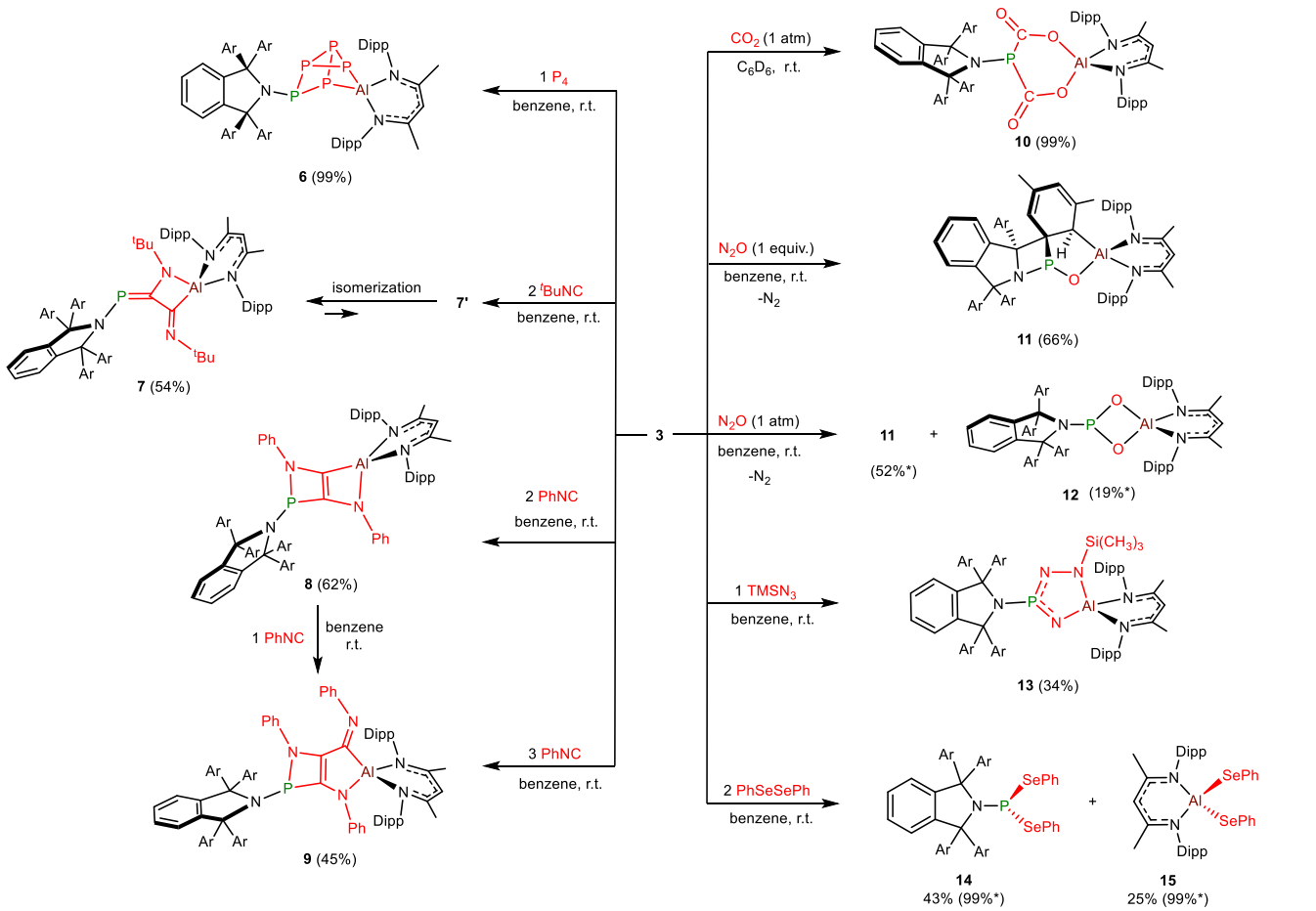

Fig. 5 | Reaction of 3 with small molecules. Components are arranged from top to bottom as P_4, isocyanides (left) and CO_2, N_2O, $TMSN_3$ and PhSeSePh (right) (*indicates NMR yield).

phosphagallene and CO_2[41,44]. It should be emphasized that when **II** reacts with CO_2, it yields a 1,3-addition product, in contrast to the total rupture of the Al = P bond seen in **3**. To further elucidate the reaction of compound **3** with CO_2, the corresponding mechanism was investigated by theoretical studies (Fig. S165).

3 was also able to activate N_2O, enable the oxidation and rupture of the Al = P double bond, yielding **11** and **12** in a 2.8:1 NMR ratio (Figs. S89 and S90). Based on these results, it's reasonable to envisage that reaction of **3** with N_2O may start from the insertion of one oxygen atom into the Al = P double bond to afford a AlPO three-membered ring scaffold, valence isoelectronic analogue of oxirane. Following intramolecular [2 + 2] cycloaddition of the Al–P bond with the arene substituent leads to the formation of **11**. On the other hand, when this oxirane intermediate was reacted with another equivalent of N_2O, the $AlPO_2$ four-membered heterocycle **12** was formed. To further investigate this deoxygenation reaction, **3** was treated with an equimolar amount of N_2O, resulting exclusively in **11** in 66% isolation yield. Despite our efforts, we could not obtain **12** in its pure state, yielding only a small number of crystals. The ^{31}P NMR spectrum of **11** displayed a doublet at 158.3 ppm ($^3J_{P\text{-}H}$ = 9.5 Hz), which collapsed to singlets upon proton decoupling. In the ^{31}P NMR spectrum of **12**, a singlet was observed at 149.7 ppm. The solid-structures of **11** and **12** were unambiguously determined by SC-XRD.

Very recently, the groups of Hering-Junghans and Braunschweig disclosed the reactivity of **I** towards organoazides, which enables the formation of various four-membered AlN_2P ring systems[52]. Surprisingly, when **3** was subjected to reaction with $TMSN_3$, a five-membered AlN_3P ring (**13**) was obtained, indicative of a distinct reaction pathway compared to those reported by Hering-Junghans and Braunschweig. The ^{31}P NMR spectrum of **13** displayed a singlet at 132.0 ppm, which is significantly downfield shifted with respect to that of **3**. The structure of **13** was determined by SC-XRD to be a spirocyclic system. The five-membered AlN_3P ring in **13** is nearly planar, with the sum of internal pentagon angles of 537.9°. Notably, the phosphorus atom of **13** shows a trigonal-planar geometry (the sum of bond angles: 360.0°), which is reminiscent of those reported in the phosphorus(V) selenides[75]. The bond lengths of P1-N2 (1.534(3) Å), P1-N4 (1.568(3) Å), and N3-N4 (1.506(3) Å) fall within the typical range of P-N single and double bonds, and N-N single and double bonds, respectively, indicative of strong π-electron delocalization over the N2-P1-N4-N3 moiety.

The reactivity of **3** with homoatomic element-element bonds such as azobenzene, bis(catecholato)diboron (B_2cat_2), and PhSeSePh was also investigated. However, the reaction of **3** with azobenzene or B_2cat_2 afforded complex mixtures, and purification of these mixtures by recrystallization was unsuccessful. When **3** was treatment with two equivalents of PhSeSePh, **14** and **15** were isolated in 43% and 25% yields, respectively[55].

Reactions of 3 with $PhSiH_3$ and $PhNH_2$: π(Al = P)-Behavior

By reacting **3** with $PhSiH_3$ and $PhNH_2$, the addition of E–H bonds (E = Si, N) across the Al = P double bond was accomplished, producing silaphosphine **16** and aminophosphine **17** in yields of 56% and 82%, respectively (Fig. 7). In contrast, intermediate **II** only exhibited 1,2-addition of the Si–H bond across the P = Al bond when reacted with $PhSiH_3$, but functions like an FLP towards amines, yielding 1,3-addition products[49]. For comparison, the reaction mechanism of **3** with aniline

https://doi.org/10.1038/s41467-026-69118-4

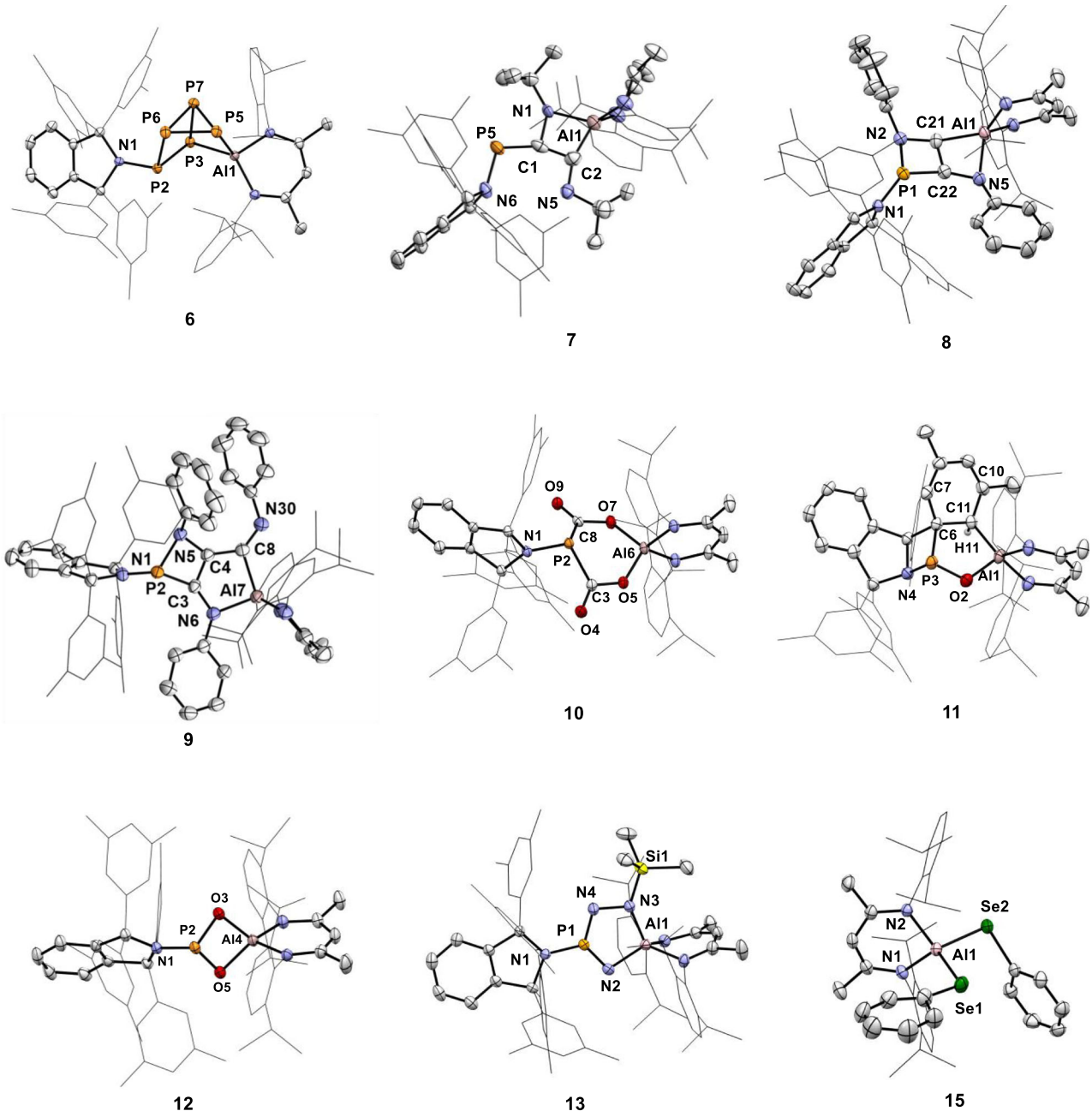

Fig. 6 | Solid-state structure of 6-15. Hydrogen atoms except that bound to C6 of **11** and solvent molecules have been omitted for clarity. Thermal ellipsoids are set at the 50% probability level.

has been studies (Fig. S166). In the ^{31}P NMR spectra, a broad doublet is observed at −81.0 ppm (d, $^{2}J_{P\text{-}H(Al)}$ = 55.4 Hz) for **16** and at −83.3 ppm (d, $^{1}J_{P\text{-}H}$ = 210.9 Hz) for **17**, with both signals collapsing to a broad singlet upon proton decoupling. The ^{1}H NMR spectrum of **16** displays a doublet in conjunction with distinct ^{29}Si satellite signals for the Si–H_2 at 4.48 ppm (d, $^{2}J_{P\text{-}H}$ = 20.0 Hz), while the Al–H resonance is not observed. For **17** the P–H resonance was observed as a doublet at 4.31 ppm (d, $^{1}J_{P\text{-}H}$ = 210.9 Hz), while the N-H resonance was identified as a singlet at 2.62 ppm. In the solid-state IR spectrum of **16**, the characteristic stretching bands for Al–H and Si–H were detected at 1871 cm^{-1} and 2130 cm^{-1}, respectively. The molecular structures of **16** and **17** were further confirmed by SC-XRD. In the solid-state structure of **16**, the Al1-P2 and P2-Si1 bond lengths (2.3924(6) and 2.2397(7) Å, respectively) are comparable to those found in a previously reported silaphosphine (Al–P: 2.37 Å, P–Si: 2.24 Å), both indicative of pronounced single bond character[47]. The Al1-P1 bond distance (2.3718(15) Å) in **17** is comparable to that found in **16**, consistent with single bond character. These isolated products clearly speak to the π(Al = P)-bonding behavior of **3**.

When **3** was reacted with styrene and 1-ethynyl-4-methylbenzene, [2 + 2] cycloaddition product **18** and **19** was formed, respectively, in addition to a small amount of C–H addition product **20** in the latter case, which are in line with those reported by Hering-Junghans and Braunschweig (Fig. 8a)[51]. However, phenylacetylene and 1-ethynyl-4-fluorobenzene, when reacted with **3**, yielded only complex mixtures, likely due to the increased acidity of their terminal alkyne C–H bond. This elevated acidity promotes alternative deprotonation or C–H activation routes, resulting in the formation of complicated mixtures instead of the intended cycloadduct. Additionally, we were unable to obtain any desired products when compound **3** reacted with

https://doi.org/10.1038/s41467-026-69118-4

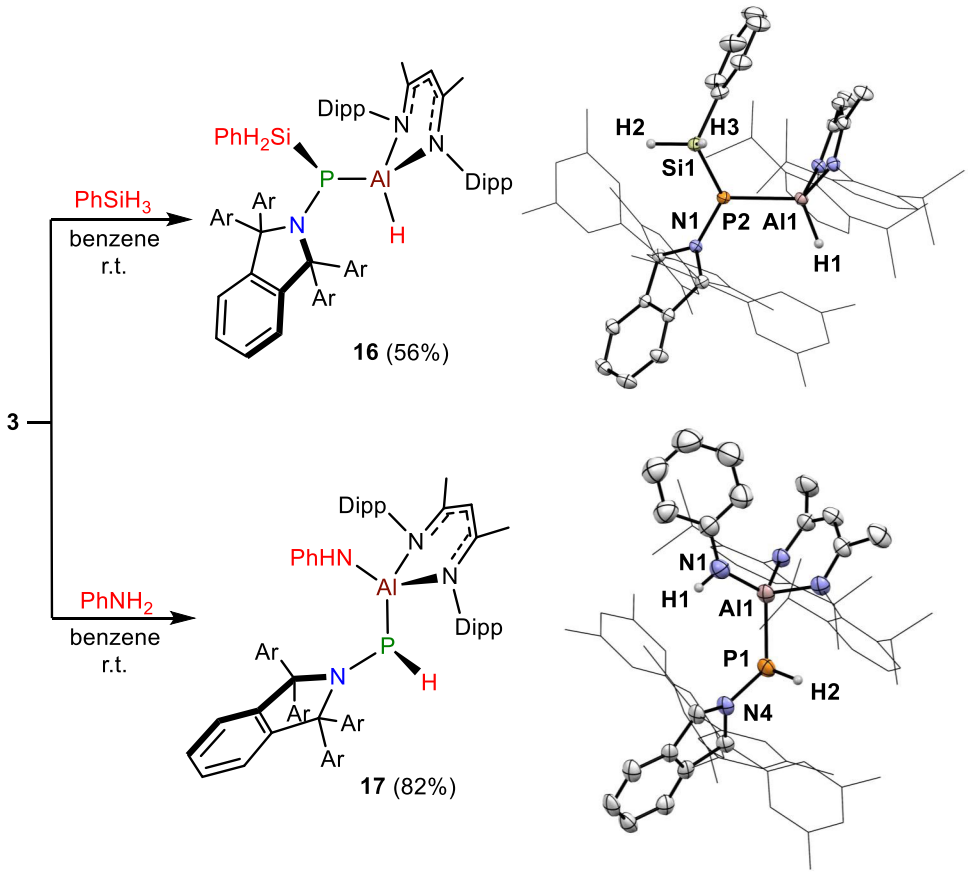

Fig. 7 | Reaction of 3 with $PhSiH_3$ and $PhNH_2$. Ellipsoids of the solid-state structures of **16** and **17** are shown at the 50% probability level. All hydrogen atoms except those bound to Si1 and Al1 of **16**, and P1 and N1 of **17**, have been omitted for clarity.

azobenzene or bis(catecholato)diboron (B_2cat_2), which might be due to uncontrolled reactions with nonpolar substrates. In the ^{31}P NMR spectra, the resonances for the phosphorus atoms in **18** and **19** were observed as a doublet of doublet at 56.7 ppm ($^2J_{P\text{-}H}$ = 35.5 Hz, $^3J_{P\text{-}H}$ = 14.7 Hz) and a doublet at 57.6 ppm ($^2J_{P\text{-}H}$ = 29.3 Hz), respectively. The ^{31}P NMR spectrum of **20** displayed a doublet at −89.3 ppm ($^1J_{P\text{-}H}$ = 204.1 Hz), which collapsed to a singlet upon proton decoupling. The solid-state structures of **18** and **19** were determined by SC-XRD, in which all four atoms of the $PAlC_2$ rings are nearly coplanar with the sums of internal tetragon angles of 358.2° and 360.0°, respectively (Fig. 8b). Unfortunately, we were unable to obtain suitable single crystals to validate the solid-structure of **20**.

In summary, by employing π-donating ^{Dipp}NacNac and isoindoline supporting ligands, a phosphaalumene(3) was successfully generated. DFT studies indicated that this phosphaalumene features a polarized Al = P double bond, with its reactivity primarily exhibiting π-character. Compound **3** is capable of activating kinetically challenging substrates, such as H_2, and reacts with P_4, isocyanides, CO_2, N_2O, $TMSN_3$, PhSeSePh, $PhSiH_3$, $PhNH_2$, styrene, and 1-ethynyl-4-methylbenzene under ambient conditions. Remarkably, **3** showcases both π(Al = P)-behavior and FLP-type reactivity with H_2, allowing 1,2-addition of H_2 across the Al = P double bond and activation of H_2 between the aluminum and pendant isoindoline substituent, respectively. Additional DFT calculations reveal that the energy barriers for these two competing pathways are close, rationalizing the concurrent observation of both reaction modes. The reaction of **3** with P_4, isocyanides, CO_2, N_2O, $TMSN_3$, or PhSeSePh proceed via complete cleavage of the Al = P bond. In addition, **3** displays distinct π(Al = P)-character in the activations of $PhSiH_3$, $PhNH_2$, styrene, and 1-ethynyl-4-methylbenzene, resulting in the cleavage of Si–H and N–H bonds, as well as the C–C unsaturated bond, across the Al = P double bond. These findings clearly demonstrate the significant π(Al = P)-character of **3**, which is notably different from the chemical behavior of **II**. This comparison underscores how the ligand environment can subtly yet significantly alter the reaction site selectivity of a P = Al bond. To gain a more profound understanding of this divergence, DFT calculations were performed. Although NBO analyses furnished valuable electronic structure insights, the NPA charges on their own did not fully explain the observed differences in reactivity, suggesting that steric effects might also play a role to some degree. Significantly, our mechanistic investigation into the reaction involving aniline uncovered distinct energy barriers for the two routes, which correlates well with our experimental findings. The crucial impact of the ligand framework provides opportunities for further research into developing reactive main-group species and ongoing investigations aim to further elucidate potential novel reactivities afforded by this unique bonding environment.

Methods

General considerations

All reactions were performed under an atmosphere of dry nitrogen or argon by using standard Schlenk or dry box techniques; solvents were dried over Na metal, K metal, or CaH_2. ^1H, ^{13}C, ^{29}Si, and ^{31}P NMR spectra were obtained with a Bruker Avance 400 spectrometer at 298 K. NMR multiplicities are abbreviated as follows: s = singlet, d = doublet, t = triplet, sep=septet, dd = doublet of doublets, ddd = doublet of doublets of doublets, qd = quartet of doublets, m = multiplet, br = broad signal. Coupling constants *J* are given in Hz. HRMS spectra were

https://doi.org/10.1038/s41467-026-69118-4

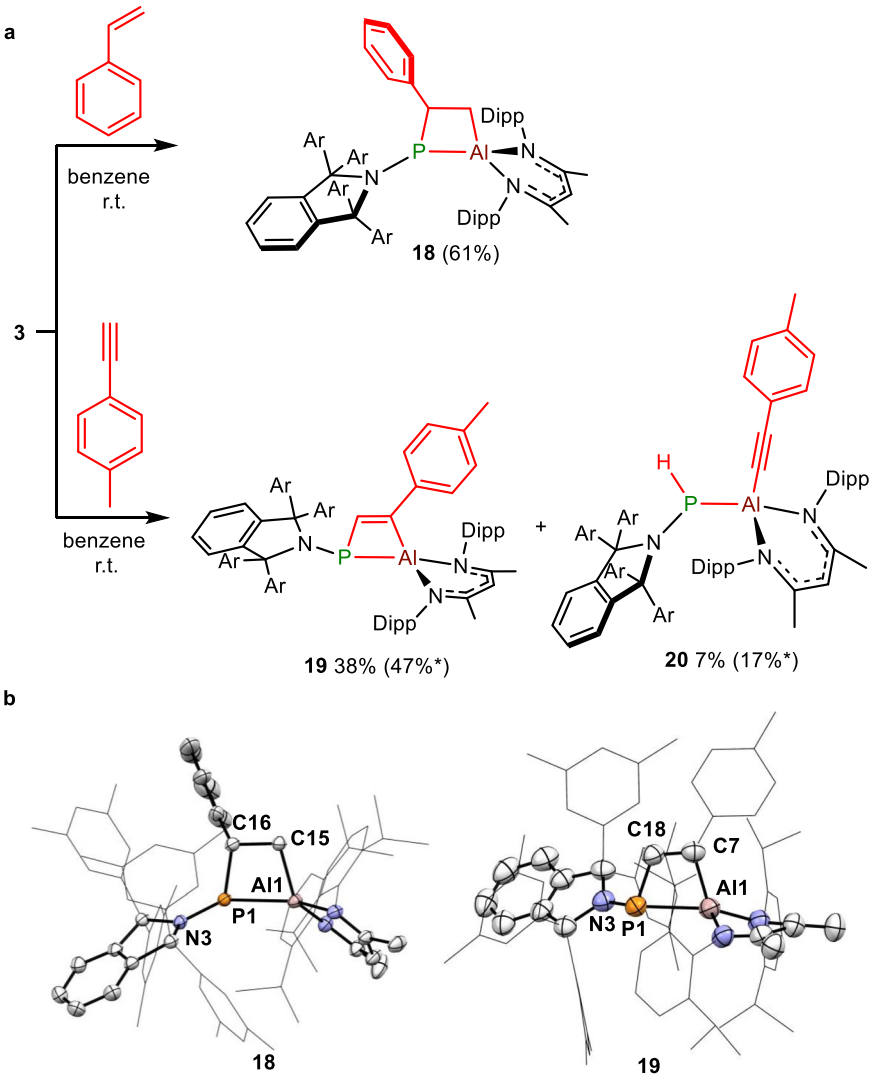

Fig. 8 | Synthesis and characterization of 18, 19, and 20. a Reaction of **3** with styrene and 1-ethynyl-4-methylbenzene (*indicates NMR yield). **b** Solid-state structure of **18** and **19** (Ellipsoids are shown at the 50% probability level. All hydrogen atoms have been omitted for clarity).

obtained from a SCIEX X500R-QTOF (ESI). Fourier transform infrared (FT-IR) spectra were recorded on a BRUKER ALPHA II spectrometer.

Synthesis of 2

At −78 °C, toluene was slowly added to a mixture of **2-Br** (3.280 × *g*, 4.52 mmol) and KC_8 (1.220 × *g*, 9.04 mmol), followed by a toluene solution of 5 eq. PMe_3 (2.6 mL, 8.7 mmol•mL^{-1}). The suspension was slowly warmed to ambient temperature and stirred in the dark overnight. Then, the mixture was filtered, and the filtrate was dried under reduced pressure. The resulting solid was washed with cold *n*-hexane (15 mL) and dried under vacuum to afford **2** as a white powder (1.510 × *g*, 52% yield). Colorless single crystals of **2** were obtained from a saturated *n*-hexane solution at −25 °C. ^{1}H NMR (400 MHz, C_6D_6, 25 °C, ppm): δ 7.46 (s, 6H, Ar-*H*), 7.23 (dd, J = 5.8, 3.2 Hz, 4H, Ar-*H*), 6.94 (dd, J = 5.8, 3.2 Hz, 2H, Ar-*H*), 6.83 (s, 4H, Ar-*H*), 2.17 (s, 24H, Ar-CH_3), 0.60 (m, 9H, PP(CH_3)$_3$). ^{13}C{^{1}H} NMR (101 MHz, C_6D_6, 25 °C, ppm): δ = 149.2 (Ar-*C*), 147.0 (Ar-*C*), 145.4 (Ar-*C*), 135.6 (Ar-*C*), 128.9 (Ar-*C*H), 128.0 (Ar-*C*H), 126.7 (Ar-*C*H), 125.7 (Ar-*C*H), 84.4 (*C*NP), 21.4 (Ar-*C*H_3), 15.9 (dd, $^1J_{P\text{-}C}$ = 30.3 Hz, $^2J_{P\text{-}C}$ = 20.2 Hz, PP(*C*H_3)$_3$). ^{31}P{^{1}H} NMR (162 MHz, C_6D_6, 25 °C, ppm): δ = −14.7 (s), −14.9 (s). ^{31}P NMR (162 MHz, C_6D_6, 25 °C, ppm): δ = −14.7 (s), −14.9 (s). FT-IR ν [cm^{-1}] 2913, 1593, 1454, 1274, 1165, 1031, 953, 847, 714, 662. HRMS (ESI): m/z calculated for $[C_{43}H_{50}NP_2]^+$ (M + H)$^+$: 642.3417; found: 642.3418.

Synthesis of 3 from 1

a): In a glove box, 20 mL of benzene was added to a mixture of ^{Dipp}NacNacM (102 mg, 0.229 mmol) and **1** (150 mg, 0.115 mmol) at ambient temperature. The reaction mixture was stirred at 50 °C for 24 h, which was accompanied by a color change from red to reddish-brown. Then all volatiles were removed under reduced pressure and the resulting mixture was dissolved in *n*-hexane. Dark-red crystals of **3** were obtained by slow evaporation of a saturated *n*-hexane solution (21 mg, 13% yield) in a glove box. ^{31}P NMR analysis indicated the formation of **3** in 42% NMR yield (PPh_3 and 1,3,5-trimethoxybenzene were used as internal standards for NMR measurements) (See Fig. S7-S8).

b): In a glove box, 20 mL of benzene was added to a mixture of ^{Dipp}NacNacM (102 mg, 0.229 mmol) and **1** (150 mg, 0.115 mmol) at ambient temperature. The reaction mixture was subjected to UV light irradiation at 365 nm overnight, which was accompanied by a color change from red to reddish-brown. Then all volatiles were removed under reduced pressure and the resulting mixture was dissolved in *n*-hexane. Dark-red crystals of **3** were obtained by slow evaporation of a saturated *n*-hexane solution in a glove box (29 mg, 18% yield). ^{31}P NMR analysis indicated the formation of **3** in 89% NMR yield. (PPh_3 and 1,3,5-trimethoxybenzene were used as internal standards for NMR measurements) (See Fig. S9-S10).

Synthesis of 3 from 2

In a glove box, **2** (433 mg, 0.675 mmol) was added to a benzene solution (20 mL) of ^{Dipp}NacNacM (300 mg, 0.675 mmol). The mixture was stirred at room temperature for 2 h, which was accompanied by a color change from red to reddish-brown. Then all volatiles were removed under reduced pressure. The resulting solid was washed with *n*-hexane (10 mL × 2) and dried under vacuum to give **3** (624 mg, 91% yield) as a red-brown powder. Dark-red single crystals of **3** were obtained by slow evaporation of a saturated *n*-hexane solution in a glove box. ^{1}H NMR (400 MHz, C_6D_6, 25 °C, ppm): δ 7.11–7.01 (m, 12H, Ar-*H*), 6.91 (d, J = 7.7 Hz, 4H, Ar-*H*), 6.82–6.74 (m, 6H, Ar-*H*), 4.80 (s, 1H, NCC*H*), 3.24 (sep, J = 6.8 Hz, 4H, C*H*CH$_3$), 2.16 (s, 24H, ArC*H*$_3$), 1.24 (s, 6H, NCC*H*$_3$), 1.23 (d, J = 6.8 Hz, 12H, CHC*H*$_3$), 1.09 (d, J = 6.8 Hz, 12H, CHC*H*$_3$). ^{13}C{^{1}H} NMR (101 MHz, C_6D_6, 25 °C, ppm): δ 171.0 (N*C*CH), 147.5 (Ar-*C*), 146.1 (Ar-*C*), 142.4 (Ar-*C*), 142.4 (d, $^{3}J_{P\text{-}C}$ = 2.8 Hz, Ar-*C*), 140.8 (d, $^{3}J_{P\text{-}C}$ = 3.8 Hz, Ar-*C*), 140.8 (Ar-*C*), 134.9 (Ar-*C*), 128.7 (d, $^{4}J_{P\text{-}C}$ = 2.5 Hz, Ar-*C*H), 128.2 (Ar-*C*H), 127.9 (Ar-*C*H), 127.5 (Ar-*C*H), 127.3 (Ar-*C*H), 126.0 (Ar-*C*H), 125.4 (Ar-*C*H), 124.1 (Ar-*C*H), 100.0 (NC*C*H), 84.6 (*C*NP), 29.1 (*C*HCH$_3$), 24.9 (CH*C*H$_3$), 23.8 (CH*C*H$_3$), 23.5 (NC*C*H$_3$), 21.7 (Ar*C*H$_3$). ^{31}P{^{1}H} NMR (162 MHz, C_6D_6, 25 °C, ppm): δ 9.0. ^{31}P NMR (162 MHz, C_6D_6, 25 °C, ppm): δ 9.0. FT-IR ν [cm^{-1}] 2952, 1594, 1518, 1435, 1372, 1318, 1248, 1008, 934, 853, 791, 728, 713, 670. HRMS (ESI): m/z calculated for [$C_{69}H_{82}AlN_3P$] $^{+}$ (M + H) $^{+}$: 1010.6057; found: 1010.6047.

Synthesis of 4 and 5

A benzene (15 mL) solution of **3** (300 mg, 0.296 mmol) in a Young-cock flask was frozen and degassed and refilled with dihydrogen gas (H_2, 1 bar). The mixture was heated at 40 °C for 12 h, which was accompanied by a color change from reddish-brown to orange. Then all volatiles were removed under reduced pressure, and the residue was recrystallized from *n*-hexane to afford **4** (65 mg, 22% yield) as colorless crystals and **5** (43 mg, 14% yield) as orange crystals, respectively. Spectroscopic data of **4**: ^{1}H NMR (400 MHz, $CDCl_3$, 25 °C, ppm): δ 7.39 (s, 1H, Ar-*H*), 7.16–7.10 (m, 2H, Ar-*H*), 6.97 - 6.86 (m, 7H, Ar-*H*), 6.74 (s, 4H, Ar-*H*), 6.69–6.64 (m, 8H, Ar-*H*), 5.14 (s, 1H, NCC*H*), 3.45 (d, $^{1}J_{P\text{-}H}$ = 204.5 Hz, 1H, P*H*), 2.98 (sep, J = 6.8 Hz, 4H, C*H*CH$_3$), 2.08 (s, 24H, Ar-C*H*$_3$), 1.53 (s, 6H, NCC*H*$_3$), 1.16 (d, J = 6.8 Hz, 6H, CHC*H*$_3$), 1.15 (d, J = 6.8 Hz, 6H, CHC*H*$_3$), 0.96 (d, J = 6.8 Hz, 6H, CHC*H*$_3$), 0.63 (d, J = 6.8 Hz, 6H, CHC*H*$_3$). ^{13}C{^{1}H} NMR (101 MHz, $CDCl_3$, 25 °C, ppm): δ 170.5 (N*C*CH), 147.0 (Ar-*C*), 145.1 (Ar-*C*), 143.8 (Ar-*C*), 143.1 (Ar-*C*), 141.4 (Ar-*C*), 135.6 (Ar-*C*), 128.8 (Ar-*C*H), 127.8 (Ar-*C*H), 126.8 (Ar-*C*H), 126.4 (Ar-*C*H), 124.7 (Ar-*C*H), 123.6 (Ar-*C*H), 98.0 (NC*C*H), 83.7 (*C*NP), 28.7 (*C*HCH$_3$), 28.6 (*C*HCH$_3$), 28.1 (NC*C*H$_3$), 24.4 (CH*C*H$_3$), 24.3 (CH*C*H$_3$), 24.1 (CH*C*H$_3$), 23.6 (CH*C*H$_3$), 21.7 (Ar*C*H$_3$). ^{31}P{^{1}H} NMR (162 MHz, $CDCl_3$, 25 °C, ppm): δ − 87.8. ^{31}P NMR (162 MHz, $CDCl_3$, 25 °C, ppm): δ − 87.8 (dd, $^{1}J_{P\text{-}H}$ = 204.5 Hz, $^{2}J_{P\text{-}H}$ = 18.6 Hz). FT-IR ν [cm^{-1}] 2961, 2916, 2863, 2244, 1834, 1594, 1522, 1436, 1385, 1318, 1252, 1165, 1017, 939, 855, 760, 712, 677, 612. HRMS (ESI): m/z calculated for [$C_{69}H_{84}AlN_3P$] $^{+}$ (M + H) $^{+}$: 1012.6213; found: 1012.6221. Spectroscopic data of **5**: ^{1}H NMR (400 MHz, C_6D_6, 25 °C, ppm): δ 7.24 (s, 4H, Ar-*H*), 7.16 (s, 3H, Ar-*H*), 7.11 (d, J = 7.9 Hz, 2H, Ar-*H*), 7.00 (d, J = 7.8 Hz, 2H, Ar-*H*), 6.96–6.86 (m, 4H, Ar-*H*), 6.82 (s, 2H, Ar-*H*), 6.74–6.56 (m, 5H, Ar-*H*), 4.93 (s, 1H, NCC*H*), 3.32 (sep, J = 6.8 Hz, 2H, C*H*CH$_3$), 3.06 (sep, J = 6.8 Hz, 2H, C*H*CH$_3$), 2.28 (s, 12H, Ar-C*H*$_3$), 2.11 (s, 12H, Ar-C*H*$_3$), 1.84 (d, $^{2}J_{P\text{-}H}$ = 5.3 Hz, 1H, N − *H*), 1.41 (s, 6H, NCC*H*$_3$), 1.10 (d, J = 6.8 Hz, 12H, CHC*H*$_3$), 1.03 (d, J = 6.8 Hz, 6H, CHC*H*$_3$). ^{13}C{^{1}H} NMR (101 MHz, C_6D_6, 25 °C, ppm): δ 170.3 (N*C*CH), 149.4 (Ar-*C*), 148.2 (Ar-*C*), 146.9 (Ar-*C*), 143.3 (Ar-*C*), 142.2 (Ar-*C*), 142.0 (Ar-*C*), 140.6 (Ar-*C*), 135.5 (Ar-*C*), 135.4 (Ar-*C*), 133.1 (Ar-*C*H), 132.2 (Ar-*C*H), 130.1 (Ar-*C*H), 127.9 (Ar-*C*H), 127.5 (Ar-*C*H), 127.2 (Ar-*C*H), 127.1 (Ar-*C*H), 125.0 (Ar-*C*H), 124.2 (Ar-*C*H), 124.0 (Ar-*C*H), 97.8 (NC*C*H), 70.8 (d, $^{2}J_{P\text{-}C}$ = 5.5 Hz, *C*NP), 57.70 (d, $^{1}J_{P\text{-}C}$ = 38.5 Hz, *C*PN), 28.3 (*C*HCH$_3$), 28.2 (*C*HCH$_3$), 24.5 (CH*C*H$_3$), 24.4 (CH*C*H$_3$), 24.1 (CH*C*H$_3$), 24.0 (CH*C*H$_3$), 23.3 (NC*C*H$_3$), 21.7 (Ar*C*H$_3$), 21.6 (Ar*C*H$_3$). ^{31}P{^{1}H} NMR (162 MHz, C_6D_6, 25 °C, ppm): δ 55.3. ^{31}P NMR (162 MHz, C_6D_6, 25 °C, ppm): δ 55.3 (d, $^{2}J_{P\text{-}H}$ = 20.1 Hz). FT-IR ν [cm^{-1}] 3347, 2962, 2920, 2865, 1817, 1592, 1522, 1439, 1380, 1320, 1254, 1178, 1100, 1018, 934, 847, 798, 762, 698, 636. HRMS (ESI): m/z calculated for [$C_{69}H_{84}AlN_3P$] $^{+}$ (M + H) $^{+}$: 1012.6213; found: 1012.6221.

Synthesis of 6

In a glove box, P_4 (12.4 mg, 0.10 mmol) was added to a benzene solution (10 mL) of **3** (101 mg, 0.10 mmol). Stirred at room temperature, the mixture gradually changed color from reddish-brown to orange over a 5-min period. The solution was dried under vacuum to afford **6** (112 mg, 99% yield) as orange powder. Orange crystals of **6** were obtained through diffusion of *n*-hexane into a saturated benzene solution at room temperature over a period of one week. ^{1}H NMR (400 MHz, C_6D_6, 25 °C, ppm): δ 7.47 (s, 4H, Ar-*H*), 7.38–7.27 (m, 6H, Ar-*H*), 7.01 (td, J = 8.0, 1.5 Hz, 3H, Ar-*H*), 6.96–6.92 (m, 2H, Ar-*H*), 6.87–6.83 (m, 4H, Ar-*H*), 6.74–6.69 (m, 3H, Ar-*H*), 4.90 (s, 1H, Ar-*H*), 3.84 (sep, J = 6.7 Hz, 1H, C*H*CH$_3$), 3.67 (sep, J = 6.7 Hz, 1H, C*H*CH$_3$), 3.28 (sep, J = 6.7 Hz, 1H, C*H*CH$_3$), 2.78 (sep, J = 6.7 Hz, 1H, C*H*CH$_3$), 2.22 (s, 12H, Ar-C*H*$_3$), 2.12 (s, 12H, Ar-C*H*$_3$), 1.74 (d, J = 6.7 Hz, 3H, CHC*H*$_3$), 1.59 (s, 3H, NCC*H*$_3$), 1.57 (s, 3H, NCC*H*$_3$), 1.35 (t, J = 6.7 Hz, 6H, CHC*H*$_3$), 1.19 (d, J = 6.7 Hz, 3H, CHC*H*$_3$), 1.09 (d, J = 6.7 Hz, 3H, CHC*H*$_3$), 1.04 (d, J = 6.7 Hz, 3H, CHC*H*$_3$), 0.97 (d, J = 6.7 Hz, 3H, CHC*H*$_3$), 0.91 (d, J = 6.7 Hz, 3H, CHC*H*$_3$). ^{13}C{^{1}H} NMR (101 MHz, C_6D_6, 25 °C, ppm): δ 172.5 (N*C*CH), 168.8 (N*C*CH), 148.9 (Ar-*C*), 146.4 (Ar-*C*), 145.7 (Ar-*C*), 144.5 (Ar-*C*), 143.7 (Ar-*C*), 142.8 (Ar-*C*), 139.0 (Ar-*C*), 137.6 (Ar-*C*), 136.2 (Ar-*C*), 135.9 (Ar-*C*), 129.9 (Ar-*C*H), 129.4 (Ar-*C*H), 129.2 (Ar-*C*H), 128.2 (Ar-*C*H), 127.8 (Ar-*C*H), 127.6 (Ar-*C*H), 127.1 (Ar-*C*H), 126.7 (Ar-*C*H), 125.0 (Ar-*C*H), 124.7 (Ar-*C*H), 124.6 (Ar-*C*H), 124.0 (Ar-*C*H), 123.7 (Ar-*C*H), 97.3 (NC*C*H), 83.8 (d, $^{2}J_{P\text{-}C}$ = 6.1 Hz, PN*C*), 29.4 (*C*HCH$_3$), 29.0 (*C*HCH$_3$), 28.7 (*C*HCH$_3$), 28.3 (*C*HCH$_3$), 25.9 (CH*C*H$_3$), 25.7 (CH*C*H$_3$), 25.4 (CH*C*H$_3$), 25.3 (CH*C*H$_3$), 25.0 (CH*C*H$_3$), 24.4 (NC*C*H$_3$), 24.3 (NC*C*H$_3$), 24.1 (CH*C*H$_3$), 24.0 (CH*C*H$_3$), 23.1 (CH*C*H$_3$), 21.7 (Ar-*C*H$_3$), 21.5 (Ar-*C*H$_3$). ^{31}P{^{1}H} NMR (162 MHz, C_6D_6, 25 °C, ppm): δ 94.5 (qd, $^{1}J_{P\text{-}P}$ = 187.9 Hz, $^{2}J_{P\text{-}P}$ = 51.8 Hz), −21.9 (dd, $^{1}J_{P\text{-}P}$ = 236.5 Hz, $^{2}J_{P\text{-}P}$ = 50.2 Hz), −81.0 (ddd, $^{1}J_{P\text{-}P}$ = 267.3 Hz, $^{2}J_{P\text{-}P}$ = 121.5 Hz, $^{3}J_{P\text{-}P}$ = 16.2 Hz), −112.8 (tt, $^{1}J_{P\text{-}P}$ = 124.8 Hz, $^{2}J_{P\text{-}P}$ = 53.5 Hz), −126.3 (dddd, $^{1}J_{P\text{-}P}$ = 265.7 Hz, $^{2}J_{P\text{-}P}$ = 139.3 Hz, $^{2}J_{P\text{-}P}$ = 124.8 Hz, $^{3}J_{P\text{-}P}$ = 21.1 Hz). ^{31}P NMR (162 MHz, C_6D_6, 25 °C, ppm): δ 94.5 (qd, $^{1}J_{P\text{-}P}$ = 187.9 Hz, $^{2}J_{P\text{-}P}$ = 51.8 Hz), −21.9 (dd, $^{1}J_{P\text{-}P}$ = 236.5 Hz, $^{2}J_{P\text{-}P}$ = 50.2 Hz), −81.0 (ddd, $^{1}J_{P\text{-}P}$ = 267.3 Hz, $^{2}J_{P\text{-}P}$ = 121.5 Hz, $^{3}J_{P\text{-}P}$ = 16.2 Hz), −112.8 (tt, $^{1}J_{P\text{-}P}$ = 124.8 Hz, $^{2}J_{P\text{-}P}$ = 53.5 Hz), −126.3 (dddd, $^{1}J_{P\text{-}P}$ = 265.7 Hz, $^{2}J_{P\text{-}P}$ = 139.3 Hz, $^{2}J_{P\text{-}P}$ = 124.8 Hz, $^{3}J_{P\text{-}P}$ = 21.1 Hz). FT-IR ν [cm^{-1}] 2964, 2916, 2865, 1592, 1528, 1437, 1385, 1315, 1254, 1168, 1010, 935, 852, 792, 719, 677. HRMS (ESI):m/z calculated for [$C_{69}H_{82}AlN_3P_5$] $^{+}$ (M + H) $^{+}$: 1134.5007; found: 1134.5000.

Synthesis of 7′

In a glove box, ^{t}BuNC (13 mg, 0.20 mmol) was added to a benzene solution (10 mL) of **3** (101 mg, 0.10 mmol). Upon addition, the mixture rapidly changed color from reddish-brown to orange at room temperature. Then all volatiles were removed under reduced pressure, and the residue was washed with *n*-hexane (5 mL × 2) to yield **7′** (89 mg, 75% yield) as an orange powder. Despite numerous attempts, obtaining single crystals of **7′** proved impossible, as **7′** underwent isomerization to **7** in solution at ambient temperature. ^{1}H NMR (400 MHz, C_6D_6, 25 °C, ppm): δ 7.34 (s, 8H, Ar-*H*), 7.15–7.09 (m, 4H, Ar-*H*), 7.06–7.03 (m, 2H, Ar-*H*), 6.99 (d, J = 1.8 Hz, 1H, Ar-*H*), 6.98 (d, J = 1.8 Hz, 1H, Ar-*H*), 6.92–6.89 (m, 2H, Ar-*H*), 6.78 (s, 4H, Ar-*H*), 4.86 (s, 1H, NCC*H*), 3.05 (sep, J = 6.7 Hz, 2H, C*H*CH$_3$), 2.98 (sep, J = 6.7 Hz, 2H, C*H*CH$_3$), 2.20 (s, 24H, ArC*H*$_3$), 1.38 (s, 6H, NCC*H*$_3$), 1.32 (s, 9H, NC(C*H*$_3$)$_3$), 1.20 (d, J = 6.7 Hz, 6H, CHC*H*$_3$), 1.17 (d, J = 6.7 Hz, 6H, CHC*H*$_3$), 1.13 (d, J = 6.7 Hz, 6H, CHC*H*$_3$), 0.95 (d, J = 6.7 Hz, 6H, CHC*H*$_3$), 0.54 (s, 9H, AlNC(C*H*$_3$)$_3$). ^{13}C{^{1}H} NMR (101 MHz, C_6D_6, 25 °C, ppm): δ 178.9 (P*C*N), 177.0 (P*C*N), 172.4 (N*C*CH), 149.5 (Ar-*C*), 145.6 (Ar-*C*), 142.4 (Ar-*C*), 139.8 (Ar-*C*), 134.8 (Ar-*C*), 130.4 (Ar-*C*H), 127.56 (Ar-*C*H), 127.5 (Ar-*C*H), 126.0 (Ar-*C*H), 125.5 (Ar-*C*H), 125.4 (Ar-*C*H), 124.0 (Ar-*C*H), 101.1 (NC*C*H), 84.9 (d, $^{2}J_{P\text{-}C}$ = 3.5 Hz, *C*NP), 55.3 (N*C*(CH$_3$)$_3$), 51.3 (N*C*(CH$_3$)$_3$), 31.0 (NC(*C*H$_3$)$_3$),

29.2 (*C*HCH$_3$), 28.6 (*C*HCH$_3$), 28.4 (CH*C*H$_3$), 26.3 (NC*C*H$_3$), 24.8 (NC(*C*H$_3$)$_3$), 24.1 (CH*C*H$_3$), 23.7 (CH*C*H$_3$), 21.6 (Ar*C*H$_3$). ^{31}P{^{1}H} NMR (162 MHz, C_6D_6, 25 °C, ppm): δ 119.3. ^{31}P NMR (162 MHz, C_6D_6, 25 °C, ppm): δ 119.3. FT-IR ν [cm^{-1}] 2964, 2916, 2865, 1592, 1533, 1436, 1376, 1279, 1017, 932, 850, 760, 716, 603. HRMS (ESI): m/z calculated for [$C_{79}H_{103}AlN_6P$]$^+$ (M + NH$_4$)$^+$: 1193.7792; found: 1193.7806.

Synthesis of 7

In a glove box, ^{t}BuNC (13 mg, 0.20 mmol) was added to a benzene solution (10 mL) of **3** (101 mg, 0.10 mmol). Upon addition, the color of the reaction mixture rapidly changed from reddish-brown to orange at room temperature. Then the mixture was heated at 60 °C for 2 days, and the color gradually changed from orange to red. Subsequently, all volatiles were removed under reduced pressure and the residue was recrystallized from *n*-hexane to afford **7** (52 mg, 44% yield) as red crystals. Single crystals of **7** were obtained by recrystallization from a saturated *n*-hexane solution at ambient temperature. ^{1}H NMR (400 MHz, C_6D_6, 25 °C, ppm): δ 7.37 (s, 8H, Ar-*H*), 7.23–7.19 (m, 2H, Ar-*H*), 7.11–7.05 (m, 4H, Ar-*H*), 7.00–6.98 (m, 2H, Ar-*H*), 6.93–6.91 (m, 2H, Ar-*H*), 6.78 (s, 4H, Ar-*H*), 5.03 (s, 1H, NCC*H*), 3.45 (sep, J = 6.7 Hz, 2H, C*H*CH$_3$), 2.93 (sep, J = 6.7 Hz, 2H, C*H*CH$_3$), 2.14 (s, 24H, ArC*H*$_3$), 1.67 (s, 9H, NC(C*H*$_3$)$_3$), 1.37 (s, 6H, NCC*H*$_3$), 1.20 (d, J = 6.7 Hz, 6H, CHC*H*$_3$), 1.12 (d, J = 6.7 Hz, 6H, CHC*H*$_3$), 1.05 (d, J = 6.7 Hz, 6H, CHC*H*$_3$), 0.94 (d, J = 6.7 Hz, 6H, CHC*H*$_3$), 0.59 (s, 9H, AlNC(C*H*$_3$)$_3$). ^{13}C{^{1}H} NMR (101 MHz, C_6D_6, 25 °C, ppm): δ 199.3 (d, $^1J_{P\text{-}C}$ = 139.1 Hz, P*C*), 171.6 (N*C*CH), 148.2 (Al*C*N), 147.4 (Ar-*C*), 145.2 (Ar-*C*), 142.9 (Ar-*C*), 140.7 (Ar-*C*), 134.7 (Ar-*C*), 130.0 (Ar-*C*H), 129.9 (Ar-*C*H), 127.7 (Ar-*C*H), 127.6 (Ar-*C*H), 125.9 (Ar-*C*H), 125.7 (Ar-*C*H), 125.5 (Ar-*C*H), 124.3 (Ar-*C*H), 102.3 (NC*C*H), 84.8 (d, $^2J_{P\text{-}C}$ = 3.1 Hz, *C*NP), 56.8 (CN*C*(CH$_3$)$_3$), 53.1 (AlN*C*(CH$_3$)$_3$), 29.8 (*C*HCH$_3$), 28.8 (*C*HCH$_3$), 28.5 (*C*HCH$_3$), 25.6 (*C*HCH$_3$), 25.0 (*C*HCH$_3$), 24.8 (NC*C*H$_3$), 24.8 (*C*HCH$_3$), 24.3 (*C*HCH$_3$), 21.6 (Ar*C*H$_3$). ^{31}P{^{1}H} NMR (162 MHz, C_6D_6, 25 °C, ppm): δ 138.9. ^{31}P NMR (162 MHz, C_6D_6, 25 °C, ppm): δ 138.9. FT-IR ν [cm^{-1}] 2962, 2921, 2865, 1594, 1526, 1461, 1376, 1311, 1242, 1199, 1163, 1107, 1012, 954, 850, 801, 709, 614. HRMS (ESI): m/z calculated for [$C_{79}H_{100}AlN_5P$]$^+$ (M + H)$^+$: 1176.7527; found: 1176.7531.

Synthesis of 8

In a glove box, PhNC (20 mg, 0.20 mmol) was added to a benzene solution (10 mL) of **3** (101 mg, 0.10 mmol). This led to a rapid color change from reddish-brown to dark red at ambient temperature. The mixture was subjected to vacuum drying and then recrystallized from *n*-hexane to afford **8** (71 mg, 62% yield) as dark red crystals. Red crystals of **8** were obtained through diffusion of *n*-hexane into a saturated benzene solution at room temperature. ^{1}H NMR (400 MHz, C_6D_6, 25 °C, ppm): δ 7.57 (s, 2H, Ar-*H*), 7.44 (s, 2H, Ar-*H*), 7.29 (s, 2H, Ar-*H*), 7.19 (s, 2H, Ar-*H*), 7.10 (s, 3H, Ar-*H*), 7.02–6.67 (m, 15H, Ar-*H*), 6.64–6.59 (m 1H, Ar-*H*), 6.45–6.35 (m, 3H, Ar-*H*), 5.96–5.93 (m, 2H, Ar-*H*), 4.92 (s, 1H, NCC*H*), 3.12 (s, 3H, C*H*CH$_3$), 2.70 (s, 1H, C*H*CH$_3$), 2.20 (s, 12H, Ar-C*H*$_3$), 2.04 (s, 6H, Ar-C*H*$_3$), 1.73 (s, 6H, Ar-C*H*$_3$), 1.46 (s, 3H, NCC*H*$_3$), 1.44 (s, 3H, CHC*H*$_3$), 1.38 (s, 3H, CHC*H*$_3$), 1.12 (s, 3H, CHC*H*$_3$), 1.03 (s, 3H, NCC*H*$_3$), 0.98 (s, 6H, CHC*H*$_3$), 0.82 (s, 3H, CHC*H*$_3$), 0.75 (s, 3H, CHC*H*$_3$), 0.43 (s, 3H, CHC*H*$_3$). ^{13}C{^{1}H} NMR (101 MHz, C_6D_6, 25 °C, ppm): δ 173.0 (N*C*CH), 170.7 (N*C*CH), 159.6 (P*C*N), 159.0 (Al*C*N), 150.3 (Ar-*C*), 148.4 (Ar-*C*), 147.9 (Ar-*C*), 145.8 (Ar-*C*), 145.7 (Ar-*C*), 145.4 (Ar-*C*), 144.9 (Ar-*C*), 144.0 (Ar-*C*), 143.0 (Ar-*C*), 142.8 (Ar-*C*), 141.3 (Ar-*C*), 139.3 (Ar-*C*), 138.7 (Ar-*C*), 137.0 (Ar-*C*), 136.5 (Ar-*C*), 136.1 (Ar-*C*), 135.0 (Ar-*C*), 129.7 (Ar-*C*H), 128.9 (Ar-*C*H), 128.8 (Ar-*C*H), 128.4 (Ar-*C*H), 127.3 (Ar-*C*H), 126.6 (Ar-*C*H), 125.7 (Ar-*C*H), 125.3 (Ar-*C*H), 125.1 (Ar-*C*H), 124.5 (Ar-*C*H), 123.6 (Ar-*C*H), 123.2 (Ar-*C*H), 118.6 (Ar-*C*H), 118.4 (Ar-*C*H), 115.1 (Ar-*C*H), 113.9 (Ar-*C*H), 98.3 (NC*C*H), 83.0 (*C*NP), 29.2 (NC*C*H$_3$), 28.0 (*C*HCH$_3$), 27.6 (*C*HCH$_3$), 25.3 (CH*C*H$_3$), 24.6 (CH*C*H$_3$), 24.1 (CH*C*H$_3$), 23.9 (CH*C*H$_3$), 23.3 (CH*C*H$_3$), 23.0 (CH*C*H$_3$), 22.2 (CH*C*H$_3$), 21.8 (Ar*C*H$_3$), 21.5 (Ar*C*H$_3$), 21.2 (Ar*C*H$_3$). ^{31}P{^{1}H} NMR (162 MHz, C_6D_6, 25 °C, ppm): δ 46.3. ^{31}P NMR (162 MHz, C_6D_6, 25 °C, ppm): δ 46.3. FT-IR ν [cm^{-1}] 2923, 2961, 2863, 1585, 1529, 1492, 1378, 1313, 1250, 1170, 1020, 1061, 939, 860, 801, 760, 690, 646. HRMS (ESI): m/z calculated for [$C_{83}H_{92}AlN_5P$]$^+$ (M + H)$^+$: 1126.6901; found: 1126.6904.

Synthesis of 9

In a glove box, PhNC (31 mg, 0.30 mmol) was added to a benzene solution (5 mL) of **3** (101 mg, 0.10 mmol). Immediately upon addition, the color of the mixture rapidly changed from reddish-brown to red at room temperature. Then the mixture was dried under vacuum and recrystallized from *n*-hexane to afford **9** (59 mg, 45% yield) as red crystals. Red single crystals of **9** were obtained by recrystallization from a saturated *n*-hexane solution at ambient temperature. ^{1}H NMR (400 MHz, $CDCl_3$, 25 °C, ppm): δ 7.36–7.27 (m, 2H, Ar-*H*), 7.24 6–7.20 (m, 3H, Ar-*H*), 7.17–7.10 (m, 7H, Ar-*H*), 7.03 (s, 2H, Ar-*H*), 6.98 (d, J = 7.5 Hz, 1H, Ar-*H*), 6.93–6.88 (m, 6H, Ar-*H*), 6.59 (d, J = 7.1 Hz, 1H, Ar-*H*), 6.53–6.46 (m, 6H, Ar-*H*), 6.43 (t, J = 6.6 Hz, 2H, Ar-*H*), 6.38–6.34 (m, 1H, Ar-*H*), 6.25 (t, J = 7.5 Hz, 2H, Ar-*H*), 5.73 (d, J = 7.6 Hz, 2H, Ar-*H*), 5.64 (s, 1H, NCC*H*), 5.54 (d, J = 7.6 Hz, 2H, Ar-*H*), 3.54 (sep, J = 6.7 Hz, 1H, C*H*CH$_3$), 3.07 (sep, J = 6.7 Hz, 1H, C*H*CH$_3$), 2.90 (sep, J = 6.7 Hz, 1H, C*H*CH$_3$), 2.66 (sep, J = 6.7 Hz, 1H, C*H*CH$_3$), 2.36 (s, 6H, Ar-C*H*$_3$), 2.03 (s, 6H, Ar-C*H*$_3$),1.90 (s, 6H, Ar-C*H*$_3$), 1.88 (s, 6H, NCC*H*$_3$), 1.82 (s, 6H, ArC*H*$_3$), 1.50 (d, J = 6.7 Hz, 3H, CHC*H*$_3$), 1.20 (d, J = 6.7 Hz, 3H, CHC*H*$_3$), 1.11 (d, J = 6.7 Hz, 3H, CHC*H*$_3$), 1.10 (d, J = 6.7 Hz, 3H, CHC*H*$_3$), 0.96 (d, J = 6.7 Hz, 3H, CHC*H*$_3$), 0.95 (d, J = 6.7 Hz, 3H, CHC*H*$_3$), 0.62 (d, J = 6.7 Hz, 3H, CHC*H*$_3$), 0.29 (d, J = 6.7 Hz, 3H, CHC*H*$_3$). ^{13}C{^{1}H} NMR (101 MHz, $CDCl_3$, 25 °C, ppm): δ 172.8 (N*C*CH), 171.4 (N*C*CH), 155.8 (d, $^1J_{P\text{-}C}$ = 34.7 Hz, P*C*C), 153.8 (Ar-*C*), 149.5 (Ar-*C*), 147.3 (Ar-*C*), 146.9 (Ar-*C*), 146.4 (Ar-*C*), 145.9 (Ar-*C*), 145.0 (Ar-*C*), 144.8 (Ar-*C*), 144.6 (Ar-*C*), 144.5 (Ar-*C*), 144.4 (Ar-*C*), 143.8 (Ar-*C*), 140.2 (Ar-*C*), 139.6 (Ar-*C*), 136.6 (Ar-*C*), 136.1 (Ar-*C*), 135.6 (Ar-*C*), 130.4 (Ar-*C*H), 130.0 (Ar-*C*H), 129.7 (Ar-*C*H), 129.6 (Ar-*C*H), 129.4 (Ar-*C*H), 129.0 (Ar-*C*H), 128.5 (Ar-*C*H), 128.1 (Ar-*C*H), 127.8 (Ar-*C*H), 127.7 (Ar-*C*H), 127.5 (Ar-*C*H), 127.1 (Ar-*C*H), 126.8 (Ar-*C*H), 126.6 (Ar-*C*H), 126.4 (Ar-*C*H), 126.3 (Ar-*C*H), 125.5 (Ar-*C*H), 125.0 (Ar-*C*H), 124.3 (Ar-*C*H), 124.1 (Ar-*C*H), 123.9 (Ar-*C*H), 122.4 (Ar-*C*H), 120.2 (Ar-*C*H), 119.9 (Ar-*C*H), 117.6 (Ar-*C*H), 117.1 (Ar-*C*H), 116.4 (Ar-*C*H), 99.6 (NC*C*H), 84.9 (d, $^2J_{P\text{-}C}$ = 28.4 Hz, CNP), 84.0 (d, $^2J_{P\text{-}C}$ = 13.6 Hz, CNP), 29.9 (*C*HCH$_3$), 29.0 (*C*HCH$_3$), 27.9 (*C*HCH$_3$), 27.6 (*C*HCH$_3$), 25.9 (CH*C*H$_3$), 25.8 (CH*C*H$_3$), 25.5 (CH*C*H$_3$), 25.0 (CH*C*H$_3$), 24.6 (CH*C*H$_3$), 24.5 (CH*C*H$_3$), 24.4 (CH*C*H$_3$), 24.2 (NC*C*H$_3$), 23.9 (NC*C*H$_3$), 23.6 (CH*C*H$_3$), 23.3 (CH*C*H$_3$), 22.0 (Ar*C*H$_3$), 21.9 (Ar*C*H$_3$), 21.4 (Ar*C*H$_3$), 21.1 (Ar*C*H$_3$). ^{31}P{^{1}H} NMR (162 MHz, $CDCl_3$, 25 °C, ppm): δ 112.0. ^{31}P NMR (162 MHz, $CDCl_3$, 25 °C, ppm): δ 112.0. FT-IR ν [cm^{-1}] 2960, 2920, 2867, 1681, 1701, 1382, 1590, 1539, 1467, 1314, 1252, 1195, 1019, 861, 800, 721, 674. HRMS (ESI): m/z calculated for [$C_{90}H_{100}AlN_7P$]$^+$ (M + NH$_4$)$^+$: 1336.7588; found: 1336.7581.

Synthesis of 10

A C_6D_6 (0.6 mL) solution of **3** (50 mg, 0.05 mmol) in a J-Young NMR tube was frozen, degassed, and charged with CO_2 (1 atm). At room temperature, the reaction mixture was shaken several times, and a rapid color change from reddish-brown to pale yellow was observed. Then all volatiles were removed under reduced pressure to give **10** (55 mg, 99% yield) as a yellow solid. Colorless crystals of **10** were obtained by recrystallization from a saturated *n*-hexane solution at ambient temperature. ^{1}H NMR (400 MHz, C_6D_6, 25 °C, ppm): δ 7.26 (d, J = 1.6 Hz, 8H, Ar-*H*), 7.20 (t, J = 7.7 Hz, 2H, Ar-*H*), 7.12–7.04 (m, 6H, Ar-*H*), 6.95 (m, 2H, Ar-*H*), 6.66 (s, 4H, Ar-*H*), 4.90 (s, 1H, NCC*H*), 2.99 (sep, J = 6.8 Hz, 4H, C*H*CH$_3$), 2.08 (s, 24H, Ar-C*H*$_3$), 1.45 (s, 6H, NCC*H*$_3$), 1.31 (d, J = 6.8 Hz, 12H, CHC*H*$_3$), 1.00 (d, J = 6.8 Hz, 12H, CHC*H*$_3$). ^{13}C{^{1}H} NMR (101 MHz, C_6D_6, 25 °C, ppm): δ 173.7 (d, $^1J_{P\text{-}C}$ = 21.0 Hz, P*C*O), 173.0 (N*C*CH), 147.8 (Ar-*C*), 144.8 (Ar-*C*), 144.3 (Ar-*C*), 136.5 (Ar-*C*), 135.4 (Ar-*C*), 129.4 (Ar-*C*H), 128.5 (Ar-*C*H), 128.3 (Ar-*C*H), 126.3 (Ar-*C*H), 125.8 (Ar-*C*H), 124.7 (Ar-*C*H), 97.5 (NC*C*H), 83.0 (*C*NP), 28.3 (*C*HCH$_3$), 24.9 (CH*C*H$_3$), 24.6 (CH*C*H$_3$), 22.9 (NC*C*H$_3$), 21.4 (Ar*C*H$_3$). ^{31}P{^{1}H} NMR (162 MHz, C_6D_6, 25 °C, ppm): δ 21.8. ^{31}P NMR (162 MHz, C_6D_6, 25 °C, ppm): δ 21.8. FT-IR ν [cm^{-1}] 2960, 2922, 2869, 1701, 1677, 1594, 1533,

1441, 1382, 1316, 1252, 1195, 1086, 1027, 883, 798, 723, 696, 662. HRMS (ESI): m/z calculated for $[C_{71}H_{81}AlO_4N_3PNa]^+$ $(M+Na)^+$: 1120.5673; found: 1120.5689.

Synthesis of 11

A benzene (5 mL) solution of **3** (101 mg, 0.10 mmol) in a Young-cock flask was injected with 2.5 mL of N_2O gas (25 °C, 1 atm, 0.10 mmol) using a syringe. The reaction mixture rapidly shifted color from reddish-brown to yellow upon introduction of N_2O gas. Then all volatiles were removed under reduced pressure and recrystallized from *n*-hexane to afford **11** (68 mg, 66% yield) as colorless crystals. ^{1}H NMR (400 MHz, C_6D_6, 25 °C, ppm): δ 7.91–7.85 (m, 1H, Ar-*H*), 7.68–7.66 (m, 1H, Ar-*H*), 7.54 (s, 2H, Ar-*H*), 7.52 (s, 1H, Ar-*H*), 7.41 (s, 2H, Ar-*H*), 7.34 (t, J = 7.7 Hz, 1H, Ar-*H*), 7.15–7.11 (m, 2H, Ar-*H*), 7.08–7.06 (m, 3H, Ar-*H*), 6.99–6.93 (m, 3H, Ar-*H*), 6.80 (s, 1H, Ar-*H*), 6.69 (s, 1H, Ar-*H*), 6.38 (s, 1H, Ar-*H*), 5.11 (m, $^3J_{P\text{-}H}$ = 9.5 Hz, 1H, PCC*H*), 5.09 (s, 1H, MeCC*H*), 4.89 (s, 1H, NCC*H*), 3.74 (sep, J = 6.8 Hz, 1H, C*H*CH$_3$), 3.11 (sep, J = 6.8 Hz, 2H, C*H*CH$_3$), 2.82 (sep, J = 6.8 Hz, 1H, C*H*CH$_3$), 2.20 (s, 6H, Ar-CH_3), 2.18 (s, 6H, Ar-CH_3), 2.04 (d, J = 6.8 Hz, 3H, CHCH_3), 2.01 (s, 6H, Ar-CH_3), 1.84 (s, 1H, AlC*H*), 1.58 (s, 3H, PCCCH_3), 1.55 (s, 3H, AlCHCCH_3), 1.35 (s, 6H, NCCH_3), 1.30 (d, J = 6.8 Hz, 3H, CHCH_3), 1.25 (d, J = 6.8 Hz, 3H, CHCH_3), 1.23 (d, J = 6.8 Hz, 3H, CHCH_3), 1.02 (d, J = 6.8 Hz, 3H, CHCH_3), 0.95 (d, J = 6.8 Hz, 3H, CHCH_3), 0.93 (d, J = 6.8 Hz, 3H, CHCH_3), 0.88 (d, J = 6.8 Hz, 3H, CHCH_3). ^{13}C{^{1}H} NMR (101 MHz, C_6D_6, 25 °C, ppm): δ 172.1 (N*C*CH), 170.8 (N*C*CH), 148.9 (Ar-*C*), 147.2 (Ar-*C*), 147.0 (Ar-*C*), 146.4 (Ar-*C*), 145.7 (Ar-*C*), 144.8 (Ar-*C*), 143.2 (Ar-*C*), 142.5 (Ar-*C*), 141.6 (Ar-*C*), 141.6 (Ar-*C*), 140.9 (Ar-*C*), 140.8 (Ar-*C*), 140.6 (Ar-*C*), 140.2 (Ar-*C*), 136.0 (Ar-*C*), 135.6 (Ar-*C*), 134.9 (Ar-*C*), 129.4 (Ar-*C*H), 129.3 (Ar-*C*H), 129.0 (Ar-*C*), 129.0 (Ar-*C*), 128.3 (Ar-*C*H), 127.8 (Ar-*C*H), 127.6 (Ar-*C*H), 127.5 (Ar-*C*H), 127.5 (Ar-*C*H), 126.7 (Ar-*C*H), 126.4 (Ar-*C*H), 125.7 (Ar-*C*H), 125.6 (Ar-*C*H), 125.1 (Ar-*C*H), 124.6 (Ar-*C*H), 124.5 (Ar-*C*H), 124. (Ar-*C*H)1, 123.2 (Ar-*C*H), 120.5 (Ar-*C*H), 120.2 (Ar-*C*H), 116.9 (Ar-*C*H), 98.2 (NC*C*H), 89.0 (d, $^2J_{P\text{-}C}$ = 4.4 Hz, PN*C*), 80.1 (d, $^2J_{P\text{-}C}$ = 20.8 Hz, PC*C*N), 49.1 (d, $^1J_{P\text{-}C}$ = 14.9 Hz, P-*C*), 29.3 (*C*HCH$_3$), 28.4 (*C*HCH$_3$), 28.3 (*C*HCH$_3$), 27.7 (Al-*C*H), 26.8 (*C*HCH$_3$), 26.0 (NC*C*H$_3$), 25.8 (NC*C*H$_3$), 25.2 (CH*C*H$_3$), 25.0 (CH*C*H$_3$), 24.9 (CH*C*H$_3$), 24.4 (CH*C*H$_3$), 24.3 (CH*C*H$_3$), 24.2 (CH*C*H$_3$), 24.1 (CH*C*H$_3$), 24.1 (CH*C*H$_3$), 23.8 (Ar*C*H$_3$), 21.7 (Ar*C*H$_3$), 21.5 (Ar*C*H$_3$), 21.5 (Ar*C*H$_3$), 21.2 (Ar*C*H$_3$). ^{31}P{^{1}H} NMR (162 MHz, C_6D_6, 25 °C, ppm): δ 158.3. ^{31}P NMR (162 MHz, C_6D_6, 25 °C, ppm): δ 158.3 (d, $^3J_{P\text{-}H}$ = 9.5 Hz). FT-IR ν [cm^{-1}] 3017, 2926, 2962, 2869, 2363, 2161, 1590, 1536, 1434, 1388, 1313, 1250, 1170, 1025, 935, 843, 794, 755, 675. HRMS (ESI): m/z calculated for $[C_{69}H_{82}AlN_3OP]^+$ $(M+H)^+$: 1026.6006; found: 1026.6005.

Synthesis of 11 and 12

A benzene (10 mL) solution of **3** (202 mg, 0.2 mmol) in a Young-Cock flask was frozen, degassed, and refilled with N_2O gas (1 atm). As the reaction mixture equilibrated to room temperature, its color gradually changed from reddish-brown to orange. The reaction mixture was then dried under vacuum to afford a mixture of **11** and **12** as an orange powder. Colorless crystals of **11** and **12** were obtained from *n*-hexane and benzene solutions at ambient temperature, respectively. However, all attempts to separate the two compounds were unsuccessful. ^{1}H and ^{31}P NMR analysis indicated the formation of **11** and **12** in 52% and 19% NMR yield, respectively. (PPh_3 and 1,3,5-Trimethoxybenzene were used as internal standards for NMR measurements) (Figs. S95–S96). Spectroscopic data of **12**: ^{31}P NMR (162 MHz, C_6D_6, 25 °C, ppm): δ 149.7. HRMS (ESI): m/z calculated for $[C_{69}H_{82}AlN_3O_2P]^+$ $(M+H)^+$: 1042.5955; found: 1042.5954.

Synthesis of 13

In a glove box, **3** (101 mg, 0.10 mmol) was added to a benzene solution (10 mL) of $TMSN_3$ (12 mg, 0.10 mmol). The mixture was stirred at room temperature overnight, with the color gradually changing from reddish-brown to orange. Following removal of all volatiles under reduced pressure, the mixture was recrystallized from *n*-hexane to afford **13** (38 mg, 34% yield) as orange crystals. Single crystals of **13** were obtained by recrystallization from a saturated *n*-hexane solution at ambient temperature. ^{1}H NMR (400 MHz, C_6D_6, 25 °C, ppm): δ 7.29–7.24 (m, 8H, Ar-*H*), 7.14 (d, J = 7.5 Hz, 2H, Ar-*H*), 7.08–7.01 (m, 4H, Ar-*H*), 6.88 - 6.85 (m, 2H, Ar-*H*), 6.79–6.73 (m, 6H, Ar-*H*), 4.96 (s, 1H, NCC*H*), 3.63 (sep, J = 6.8 Hz, 2H, C*H*CH$_3$), 3.12 (sep, J = 6.8 Hz, 2H, C*H*CH$_3$), 2.04 (s, 24H, ArCH_3), 1.30 (s, 6H, NCCH_3), 1.26 (d, J = 6.8 Hz, 6H, CHCH_3), 1.15 (d, J = 6.8 Hz, 6H, CHCH_3), 1.12 (d, J = 6.8 Hz, 6H, CHCH_3), 0.93 (d, J = 6.8 Hz, 6H, CHCH_3), 0.27 (s, 9H, Si(CH_3)$_3$). ^{13}C{^{1}H} NMR (101 MHz, C_6D_6, 25 °C, ppm): δ 170.1 (N*C*CH), 145.8 (Ar-*C*), 145.7 (Ar-*C*), 145.5 (Ar-*C*), 144.0 (Ar-*C*), 143.7 (Ar-*C*), 141.2 (Ar-*C*), 135.7 (Ar-*C*), 128.6 (Ar-*C*H), 128.5 (Ar-*C*H), 127.1 (Ar-*C*H), 127.1 (Ar-*C*H), 124.7 (Ar-*C*H), 124.1 (Ar-*C*H), 123.9 (Ar-*C*H), 100.6 (NC*C*H), 82.2 (d, $^2J_{P\text{-}C}$ = 3.1 Hz, *C*NP), 28.3 (NC*C*H$_3$), 27.6 (*C*HCH$_3$), 25.3 (CH*C*H$_3$), 24.1 (CH*C*H$_3$), 23.6 (CH*C*H$_3$), 23.5 (CH*C*H$_3$), 21.5 (Ar*C*H$_3$), 1.2 (Si(*C*H$_3$)$_3$). ^{31}P{^{1}H} NMR (162 MHz, C_6D_6, 25 °C, ppm): δ 132.0. ^{31}P NMR (162 MHz, C_6D_6, 25 °C, ppm): δ 132.0. FT-IR ν [cm^{-1}] 3017, 2961, 2923, 2867, 1594, 1539, 1462, 1379, 1318, 1233, 1194, 1126, 1020, 966, 835, 799, 704, 666. HRMS (ESI): m/z calculated for $[C_{72}H_{91}AlN_6PSi]^+$ $(M+H)^+$: 1125.6622; found: 1125.6625.

Synthesis of 14 and 15

In a glove box, **3** (101 mg, 0.10 mmol) was added to a benzene solution (10 mL) of PhSeSePh (61 mg, 0.20 mmol). The mixture was stirred at room temperature overnight, with the color gradually changing from reddish-brown to yellow. Then all volatiles were removed under reduced pressure, and the resulting mixture was recrystallized from *n*-hexane to afford **14**[55] (38 mg, 43% yield) and **15** (16 mg, 25% yield) as colourless crystals. Single crystals of **15** were obtained by recrystallization from a saturated *n*-hexane solution at ambient temperature. ^{31}P and ^{1}H NMR analysis confirmed the formation of **14** and **15** with NMR yields of 99% and 99%, respectively. (PPh_3 and 1,3,5-trimethoxybenzene were used as internal standards for NMR measurements) (For NMR spectra of the reaction mixture, see Figs. S104 and105). Spectroscopic data of **15**: ^{1}H NMR (400 MHz, C_6D_6, 25 °C, ppm): δ 7.24–7.17 (m, 5H, Ar-*H*), 7.14 (d, J = 5.9 Hz, 5H, Ar-*H*), 6.92–6.81 (m, 6H, Ar-*H*), 5.07 (s, 1H, NCC*H*), 3.41 (sep, J = 6.8 Hz, 4H, C*H*CH$_3$), 1.49 (s, 6H, NCCH_3), 1.44 (d, J = 6.8 Hz, 12H, CHCH_3), 1.00 (d, J = 6.8 Hz, 12H, CHCH_3). ^{13}C{^{1}H} NMR (101 MHz, C_6D_6, 25 °C, ppm): δ 171.7 (N*C*CH), 144.8 (Ar-*C*), 140.0 (Ar-*C*), 136.0 (Ar-*C*), 129.2 (Ar-*C*H), 128.1 (Ar-*C*H), 127.8 (Ar-*C*H), 124.8 (Ar-*C*H), 124.8 (Ar-*C*H), 99.5 (NC*C*H), 28.6 (*C*HCH$_3$), 25.2 (CH*C*H$_3$), 24.7 (CH*C*H$_3$), 23.7 (NC*C*H$_3$). FT-IR ν [cm^{-1}] 3058, 2957, 2925, 2865, 1575, 1526, 1436, 1364, 1313, 1243, 1175, 1100, 1019, 934, 877, 797, 729, 685. HRMS (ESI): m/z calculated for $[C_{41}H_{52}AlN_2Se_2]^+$ $(M+H)^+$: 759.2271; found: 759.2270.

Synthesis of 16

$PhSiH_3$ (11 mg, 0.10 mmol) was added to a benzene solution (10 mL) of 3 (101 mg, 0.10 mmol) at room temperature. Upon addition, the mixture rapidly changed color from reddish-brown to yellow. Following removal of all volatiles under reduced pressure, the resulting mixture was recrystallized from *n*-hexane to afford **16** (64 mg, 56% yield) as yellow crystals. Single crystals of **16** were obtained by recrystallization from a saturated *n*-hexane solution at ambient temperature. ^{1}H NMR (400 MHz, C_6D_6, 25 °C, ppm): δ 7.77–7.74 (m, 2H, Ar-*H*), 7.47 (s, 4H, Ar-*H*), 7.14–7.07 (m, 14H, Ar-*H*), 6.94 (dd, J = 5.9, 3.2 Hz, 2H, Ar-*H*), 6.86 (s, 2H, Ar-*H*), 6.72–6.69 (m, 4H, Ar-*H*), 4.48 (d, $^2J_{P\text{-}H}$ = 20.0 Hz, 2H, SiH_2), 4.11 (s, 1H, NCC*H*), 3.51 (sep, J = 6.7 Hz, 2H, C*H*CH$_3$), 3.16 (sep, J = 6.7 Hz, 2H, C*H*CH$_3$), 2.26 (s, 12H, Ar-CH_3), 1.77 (s, 12H, Ar-CH_3), 1.33 (d, J = 6.7 Hz, 6H, CHCH_3), 1.20 (d, J = 6.7 Hz, 6H, CHCH_3), 1.10 (s, 6H, NCCH_3), 1.00 (d, J = 6.7 Hz, 6H, CHCH_3), 0.99 (d, J = 6.7 Hz, 6H, CHCH_3). ^{13}C{^{1}H} NMR (101 MHz, C_6D_6, 25 °C, ppm): δ 170.0 (N*C*CH), 147.4 (d, $J_{P\text{-}C}$ = 3.8 Hz, Ar-*C*), 147.3 (Ar-*C*), 145.9 (Ar-*C*), 144.1 (Ar-*C*), 142.8 (Ar-*C*), 136.8 (Ar-*C*), 136.6 (d, $J_{P\text{-}C}$ = 3.3 Hz, Ar-*C*H), 136.2 (Ar-*C*), 129.7 (Ar-*C*H), 128.8 (Ar-*C*H), 128.5 (Ar-*C*H), 127.8 (Ar-*C*H), 127.6 (Ar-*C*H), 127.2 (Ar-*C*H),

126.4 (Ar-*C*H), 125.3 (Ar-*C*H), 125.0 (Ar-*C*H), 124.9 (Ar-*C*H), 100.2 (NC*C*H), 84.7 (d, $J_{P\text{-}C}$ = 2.2 Hz, *C*NP), 28.3 (*C*HCH$_3$), 27.8 (d, $J_{P\text{-}C}$ = 3.8 Hz, *C*HCH$_3$), 26.6 (NC*C*H$_3$), 24.9 (*C*HCH$_3$), 24.9 (CH*C*H$_3$), 24.8 (CH*C*H$_3$), 24.6 (CH*C*H$_3$), 21.2 (Ar*C*H$_3$). ^{31}P{^{1}H} NMR (162 MHz, C$_6$D$_6$, 25 °C, ppm): δ − 81.0. ^{31}P NMR (162 MHz, C$_6$D$_6$, 25 °C, ppm): δ − 81.0 (d, $^2J_{P\text{-}H}$ = 55.4 Hz). ^{29}Si NMR (79 MHz, C$_6$D$_6$, 25 °C, ppm) δ − 35.60 (d, $^1J_{P\text{-}Si}$ = 42.0 Hz). FT-IR ν [cm^{-1}] 2958, 2920, 2865, 2130, 1871, 1594, 1514, 1463, 1390, 1308, 1244, 1163, 1104, 1031, 961, 853, 800, 700. HRMS (ESI): m/z calculated for [C$_{75}$H$_{89}$AlN$_3$PSiNa]$^+$ (M+Na)$^+$: 1140.6271; found: 1140.6271.

Synthesis of 17

In a glove box, **3** (101 mg, 0.10 mmol) was added to a benzene solution (10 mL) of PhNH$_2$ (9 mg, 0.10 mmol). Upon addition of the substrate, the mixture rapidly changed color from reddish-brown to yellow at room temperature. Then all volatiles were removed under reduced pressure and washed with *n*-hexane (5 mL × 2) to yield **17** (91 mg, 82% yield) as a white powder. Colorless crystals of **17** were obtained by recrystallization from a mixture of *n*-hexane and benzene at ambient temperature. ^{1}H NMR (400 MHz, C$_6$D$_6$, 25 °C, ppm): δ 7.28–7.23 (m, 2H, Ar-*H*), 7.12 (s, 8H, Ar-*H*), 7.09–7.07 (m, 2H, Ar-*H*), 6.94 (d, *J* = 7.7 Hz, 4H, Ar-*H*), 6.84 (s, 4H, Ar-*H*), 6.76 (d, *J* = 7.2 Hz, 1H, Ar-*H*), 6.70 (d, *J* = 2.5 Hz, 3H, Ar-*H*), 6.63 (d, *J* = 8.0 Hz, 2H, Ar-*H*), 6.35 (d, *J* = 7.5 Hz, 1H, Ar-*H*), 5.19 (s, 1H, NCC*H*), 4.31 (d, $^1J_{P\text{-}H}$ = 210.9 Hz, 1H, P-*H*), 3.26 (sep, *J* = 6.7 Hz, 2H, C*H*CH$_3$), 3.09 (sep, *J* = 6.7 Hz, 2H, C*H*CH$_3$), 2.62 (s, 1H, N-*H*), 2.11 (s, 24H, Ar-C*H*$_3$), 1.40 (d, *J* = 6.7 Hz, 6H, CHC*H*$_3$), 1.30 (s, 6H, NCC*H*$_3$), 1.03 (d, *J* = 6.7 Hz, 6H, CHC*H*$_3$), 1.01 (d, *J* = 6.7 Hz, 6H, CHC*H*$_3$), 0.91 (d, *J* = 6.7 Hz, 6H, CHC*H*$_3$). ^{13}C{^{1}H} NMR (101 MHz, C$_6$D$_6$, 25 °C, ppm): δ 170.4 (N*C*CH), 150.8 (Ar-*C*), 148.6 (d, $^2J_{P\text{-}C}$ = 4.1 Hz, Ar-*C*), 145.2 (Ar-*C*), 144.4 (Ar-*C*), 143.5 (Ar-*C*), 142.0 (Ar-*C*), 135.7 (Ar-*C*), 129.2 (Ar-*C*H), 128.2 (Ar-*C*H), 128.1 (Ar-*C*H), 127.4 (Ar-*C*H), 126.4 (Ar-*C*H), 124.5 (Ar-*C*H), 124.1 (Ar-*C*H), 123.9 (Ar-*C*H), 118.6 (Ar-*C*H), 115.2 (Ar-*C*H), 100.8 (NC*C*H), 83.4 (d, $^2J_{P\text{-}C}$ = 4.7 Hz, *C*NP), 29.1 (*C*HCH$_3$), 28.9 (*C*HCH$_3$), 27.2 (*C*HCH$_3$), 25.5 (CH*C*H$_3$), 24.9 (*C*HCH$_3$), 24.5 (*C*HCH$_3$), 24.2 (CH*C*H$_3$), 23.8 (NC*C*H$_3$), 21.8 (Ar*C*H$_3$). ^{31}P{^{1}H} NMR (162 MHz, C$_6$D$_6$, 25 °C, ppm): δ − 83.3. ^{31}P NMR (162 MHz, C$_6$D$_6$, 25 °C, ppm): δ − 83.3 (d, $^1J_{P\text{-}H}$ = 210.9 Hz). FT-IR ν [cm^{-1}] 3345, 2963, 2921, 2863, 1596, 1531, 1437, 1369, 1318, 1274, 1172, 1018, 938, 855, 798, 719. HRMS (ESI): m/z calculated for [C$_{75}$H$_{89}$AlN$_6$P]$^+$ (M + H)$^+$: 1103.6635; found: 1103.6639.

Synthesis of 18

In a glove box, **3** (100 mg, 0.10 mmol) was added to a benzene solution (10 mL) of styrene (11 mg, 0.10 mmol). The mixture was stirred at room temperature overnight, with the color gradually changing from reddish-brown to red. Then all volatiles were removed under reduced pressure and the residue was washed with *n*-hexane to afford **18** (69 mg, 61% yield) as an orange powder. Orange crystals of **18** were obtained by recrystallization from a saturated benzene solution at ambient temperature. ^{1}H NMR (400 MHz, C$_6$D$_6$, 25 °C, ppm): δ 7.50–7.18 (m, 7H, Ar-*H*), 7.15–6.66 (m, 15H, Ar-*H*), 6.59–6.31 (m, 5H, Ar-*H*), 4.83 (s, 1H, NCC*H*), 3.45–3.25 (m, 3H, C*H*CH$_3$), 3.04 (sep, *J* = 6.8 Hz, 2H, C*H*CH$_3$), 2.31 (s, 6H, Ar-C*H*$_3$), 2.24 (s, 6H, Ar-C*H*$_3$), 2.18–2.15 (m, 2H, AlC*H*$_2$), 1.97 (s, 6H, Ar-C*H*$_3$), 1.83 (s, 6H, Ar-C*H*$_3$), 1.57 (s, 3H, NCC*H*$_3$), 1.33 (s, 3H, NCC*H*$_3$), 1.27 (d, *J* = 6.8 Hz, 3H, CHC*H*$_3$), 1.14 (d, *J* = 6.8 Hz, 3H, CHC*H*$_3$), 1.10–0.96 (m, 12H, CHC*H*$_3$), 0.93 (d, *J* = 6.8 Hz, 3H, CHC*H*$_3$), 0.86 (d, *J* = 6.8 Hz, 3H, CHC*H*$_3$), 0.29 (t, *J* = 14.6 Hz, 1H, PC*H*). ^{13}C{^{1}H} NMR (101 MHz, C$_6$D$_6$, 25 °C, ppm): δ 171.9 (N*C*CH), 171.1 (N*C*CH), 153.9 (Ar-*C*), 153.7 (Ar-*C*), 148.8 (Ar-*C*), 148.2 (Ar-*C*), 147.4 (Ar-*C*), 146.8 (Ar-*C*), 145.4 (Ar-*C*), 144.2 (Ar-*C*), 143.9 (Ar-*C*), 142.9 (Ar-*C*), 142.1 (Ar-*C*), 141.6 (Ar-*C*), 136.6 (Ar-*C*), 135.8 (Ar-*C*), 135.0 (Ar-*C*), 130.5 (Ar-*C*H), 129.1 (Ar-*C*H), 128.2 (Ar-*C*H), 127.8 (Ar-*C*H), 127.6 (Ar-*C*H), 127.2 (Ar-*C*H), 126.6 (Ar-*C*H), 125.8 (Ar-*C*H), 125.1 (Ar-*C*H), 124.7 (Ar-*C*H), 123.5 (Ar-*C*H), 122.8 (Ar-*C*H), 98.5 (NC*C*H), 85.1 (*C*NP), 41.3 (d, $^1J_{P\text{-}C}$ = 24.7 Hz, P*C*H), 29.7 (CH*C*H$_3$), 29.2 (CH*C*H$_3$), 28.7 (CH*C*H$_3$), 28.1 (CH*C*H$_3$), 25.8 (AlC*H*$_2$), 25.5 (CH*C*H$_3$), 25.2 (NC*C*H$_3$), 25.1 (CH*C*H$_3$), 24.9 (CH*C*H$_3$), 24.6 (CH*C*H$_3$), 24.4 (NC*C*H$_3$), 24.0 (CH*C*H$_3$), 22.6 (CH*C*H$_3$), 21.4 (Ar*C*H$_3$). ^{31}P{^{1}H} NMR (162 MHz, C$_6$D$_6$, 25 °C, ppm): δ 56.7. ^{31}P NMR (162 MHz, C$_6$D$_6$, 25 °C, ppm): δ 56.7 (dd, $^2J_{P\text{-}H}$ = 35.5 Hz, $^3J_{P\text{-}H}$ = 14.7 Hz). FT-IR ν [cm^{-1}] 2961, 2918, 2867, 1592, 1524, 1439, 1386, 1310, 1250, 1170, 1092, 1019, 934, 850, 797, 762, 702, 675. HRMS (ESI): m/z calculated for [C$_{77}$H$_{90}$AlN$_3$P]$^+$ (M + H)$^+$: 1114.668; found: 1114.660.

Synthesis of 19 and 20

In a glove box, **3** (202 mg, 0.20 mmol) was added to a benzene solution (20 mL) of 1-ethynyl-4-methylbenzene (23 mg, 0.20 mmol). The mixture was stirred at room temperature, accompanied by a rapid color change from reddish-brown to red. Following removal of all volatiles under reduced pressure, the mixture was recrystallized successively from a mixture of *n*-hexane and benzene to afford red crystals of **19** (85 mg, 38% yield) and a small number of colorless crystals of **20** (16 mg, 7% yield), respectively. Single crystals of **19** were obtained by recrystallization from a saturated *n*-hexane solution at ambient temperature. Regrettably, we were unable to obtain single crystals of **20** that were suitable for SC-XRD analysis. ^{31}P and ^{1}H NMR analysis confirmed the formation of **19** and **20** with NMR yields of 47% and 17%, respectively. (PPh$_3$ and 1,3,5-trimethoxybenzene were used as internal standards for NMR measurements) (For NMR spectra of the reaction mixture, see Figs. S131 and S132). Spectroscopic data of **19**: ^{1}H NMR (400 MHz, C$_6$D$_6$, 25 °C, ppm): δ 8.16 (d, $^2J_{P\text{-}H}$ = 29.3 Hz, 1H, PC*H*), 7.46 (d, J = 7.7 Hz, 2H, Ar-*H*), 7.34 (s, 1H, Ar-*H*), 7.16 (s, 5H, Ar-*H*), 7.11 (d, J = 8.1 Hz, 3H, Ar-*H*), 7.08–7.02 (m, 5H, Ar-*H*), 6.90–6.88 (m, 2H, Ar-*H*), 6.86–6.83 (m, H, Ar-*H*), 6.74–6.70 (m, 6H, Ar-*H*), 5.12 (s, 1H, NCC*H*), 3.04 (sep, *J* = 6.8 Hz, 2H, C*H*CH$_3$), 3.00 (sep, *J* = 6.8 Hz, 2H, C*H*CH$_3$), 2.19 (s, 3H, Ar-C*H*$_3$), 2.16 (s, 24H, ArC*H*$_3$), 1.34 (s, 6H, NCC*H*$_3$), 1.13 (d, *J* = 6.8 Hz, 6H, CHC*H*$_3$), 1.10 (d, *J* = 6.8 Hz, 6H, CHC*H*$_3$), 0.98 (d, *J* = 6.8 Hz, 6H, CHC*H*$_3$), 0.88 (d, *J* = 6.8 Hz, 3H, CHC*H*$_3$). ^{13}C{^{1}H} NMR (101 MHz, C$_6$D$_6$, 25 °C, ppm): δ 170.5 (N*C*CH), 161.7 (d, $^1J_{P\text{-}C}$ = 22.8 Hz, P*C*HC), 148.8 (Ar-*C*), 146.0 (Ar-*C*), 144.4 (Ar-*C*), 142.0 (Ar-*C*), 141.6 (Ar-*C*), 140.6 (d, $^2J_{P\text{-}C}$ = 13.3 Hz, PCH*C*), 135.2 (Ar-*C*), 135.0 (Ar-*C*), 133.6 (Ar-*C*), 129.4 (Ar-*C*H), 128.4 (Ar-*C*H), 128.1 (Ar-*C*H), 126.9 (Ar-*C*H), 126.3 (Ar-*C*H), 124.8 (Ar-*C*H), 124.5 (Ar-*C*H), 123.7 (Ar-*C*H), 99.5 (NC*C*H), 83.5 (d, $^2J_{P\text{-}C}$ = 4.3 Hz, *C*NP), 28.3 (NC*C*H$_3$), 27.5 (*C*HCH$_3$), 25.2 (CH*C*H$_3$), 24.4 (CH*C*H$_3$), 24.0 (CH*C*H$_3$), 23.8 (CH*C*H$_3$), 21.8 (Ar*C*H$_3$), 21.0 (Ar*C*H$_3$). ^{31}P{^{1}H} NMR (162 MHz, C$_6$D$_6$, 25 °C, ppm): δ 57.6. ^{31}P NMR (162 MHz, C$_6$D$_6$, 25 °C, ppm): δ 57.6 (d, $^2J_{P\text{-}H}$ = 29.3 Hz). FT-IR ν [cm^{-1}] 3017, 2954, 2921, 2865, 1574, 1521, 1436, 1374, 1313, 1250, 1172, 1012, 937, 855, 813, 716, 643. HRMS (ESI): m/z calculated for [C$_{78}$H$_{90}$AlN$_3$P]$^+$ (M + H)$^+$: 1126.6688; found: 1126.6692. Spectroscopic data of **20**: ^{1}H NMR (400 MHz, C$_6$D$_6$, 25 °C, ppm): δ 7.55 (d, *J* = 8.0 Hz, 2H, Ar-H), 7.11 (d, *J* = 7.6 Hz, 2H, Ar-H), 7.08–7.02 (m, 10H, Ar-H), 6.98–6.91 (m, 4H, Ar-H), 6.85–6.79 (m, 6H, Ar-H), 6.72–6.69 (m, 2H, Ar-H), 4.94 (s, 1H, NCC*H*), 3.97 (d, $^1J_{P\text{-}H}$ = 204.1 Hz, 1H, P-*H*), 3.80 (sep, *J* = 6.8 Hz, 2H, C*H*CH$_3$), 3.12 (sep, *J* = 6.8 Hz, 2H, C*H*CH$_3$), 2.13 (s, 24H, ArC*H*$_3$), 2.06 (s, 3H, ArC*H*$_3$), 1.35 (d, *J* = 6.8 Hz, 6H, CHC*H*$_3$), 1.32 (d, *J* = 6.8 Hz, 6H, CHC*H*$_3$), 1.29 (s, 6H, NCC*H*$_3$), 1.03 (d, *J* = 6.8 Hz, 6H, CHC*H*$_3$), 0.98 (d, *J* = 6.8 Hz, 6H, CHC*H*$_3$). ^{13}C{^{1}H} NMR (101 MHz, C$_6$D$_6$, 25 °C, ppm): δ 170.4 (N*C*CH), 148.1 (Ar-*C*), 148.0 (Ar-*C*), 145.2 (Ar-*C*), 144.3 (Ar-*C*), 143.3 (Ar-*C*), 142.0 (Ar-*C*), 136.5 (Ar-*C*), 135.9 (Ar-*C*), 131.5 (Ar-*C*H), 129.0 (Ar-*C*H), 128.8 (Ar-*C*H), 127.0 (Ar-*C*H), 126.4 (Ar-*C*H), 124.8 (Ar-*C*H), 123.9 (AlC*C*Ar), 123.8 (Ar-*C*H), 123.7 (Ar-*C*H), 105.1 (AlC*C*Ar), 100.2 (NC*C*H), 83.7 (d, $^2J_{P\text{-}C}$ = 4.7 Hz, *C*NP), 28.6 (*C*HCH$_3$), 28.5 (*C*HCH$_3$), 28.4 (*C*HCH$_3$), 26.5 (CH*C*H$_3$), 24.9 (NC*C*H$_3$), 24.8 (NC*C*H$_3$), 24.2 (CH*C*H$_3$), 24.0 (CH*C*H$_3$), 23.7 (CH*C*H$_3$), 21.9 (Ar*C*H$_3$), 21.0 (Ar*C*H$_3$). ^{31}P{^{1}H} NMR (162 MHz, C$_6$D$_6$, 25 °C, ppm): δ − 89.5. ^{31}P NMR (162 MHz, C$_6$D$_6$, 25 °C, ppm): δ − 89.5 (d, $^1J_{P\text{-}H}$ = 204.1 Hz). FT-IR ν [cm^{-1}] 3015, 2961, 2918, 2863, 2246, 1594, 1533, 1437, 1368, 1318, 1254, 1179, 1100, 1019, 937, 852, 797, 716, 680, 646. HRMS (ESI): m/z calculated for [C$_{78}$H$_{90}$AlN$_3$P]$^+$ (M + H)$^+$: 1126.6688; found: 1126.6724.

Data availability

All data generated or analyzed during this study are included in the Supplementary Information. Details about materials and methods, experimental procedures, characterization data, and theoretical calculations are available in the Supplementary Information. The structures of **2**–**13** and **15**–**19** in the solid state were determined by single-crystal X-ray diffraction studies and the crystallographic data have been deposited with the Cambridge Crystallographic Data Center under nos. CCDC 2455485 (**2**), 2455483 (**3**), 2455486 (**4**), 2455481 (**5**), 2475851 (**6**), 2455482 (**7**), 2503430 (**8**), 2455480 (**9**), 2455487 (**10**), 2475850 (**11**), 2475849 (**12**), 2503426 (**13**), 2503427(**15**), 2455479 (**16**), 2455484 (**17**), 2503429 (**18**), and 2503428 (**19**). These data can be obtained free of charge from the Cambridge Crystallographic Data Center via www.ccdc.cam.ac.uk/data request/cif. All data are also available from corresponding authors upon request. Source data are provided with this paper.

References

1. Power, P. P. π-Bonding and the lone pair effect in multiple bonds between heavier main group elements. *Chem. Rev.* **99**, 3463–3504 (1999).
2. Fischer, R. C. & Power, P. P. π-bonding and the lone pair effect in multiple bonds involving heavier main group elements: developments in the new millennium. *Chem. Rev.* **110**, 3877–3923 (2010).
3. Bag, P., Weetman, C. & Inoue, S. Experimental realisation of elusive multiple-bonded aluminium compounds: a new horizon in aluminium chemistry. *Angew. Chem. Int. Ed.* **57**, 14394–14413 (2018).
4. Borthakur, R. & Chandrasekhar, V. Boron-Heteroelement (B–E; E = Al, C, Si, Ge, N, P, As, Bi, O, S, Se, Te) multiply bonded compounds: recent advances. *Coord. Chem. Rev.* **429**, 213647 (2021).
5. Weetman, C. Main group multiple bonds for bond activations and catalysis. *Chem. Eur. J.* **27**, 1941–1954 (2021).
6. Dankert, F. & Hering-Junghans, C. Heavier group 13/15 multiple bond systems: synthesis, structure and chemical bond activation. *Chem. Commun.* **58**, 1242–1262 (2022).
7. Paetzold, P. Iminoboranes. *Adv. Inorg. Chem.* **31**, 123–170 (1987).
8. Nöth, H. The chemistry of amino imino boranes. *Angew. Chem. Int. Ed. Engl.* **27**, 1603–1623 (1988).
9. Fan, Y., Cui, J. & Kong, L. Recent advances in the chemistry of iminoborane derivatives. *Eur. J. Org. Chem.* **43**, e202201086 (2022).
10. Linti, G., Nöth, H., Polborn, K. & Paine, R. T. An allene-analogous boranylidenephosphane with B=P double bond: 1,1-diethylpropyl(2,2,6,6-tetramethylpiperidino)- boranylidenephosphane-*P*-pentacarbonyl-chromium. *Angew. Chem. Int. Ed. Engl.* **29**, 682–684 (1990).
11. Power, P. P. Boron-phosphorus compounds and multiple bonding. *Angew. Chem. Int. Ed. Engl.* **29**, 449–460 (1990).
12. Pestana, D. C. & Power, P. P. Nature of the boron-phosphorus bond in monomeric phosphinoboranes and related compounds. *J. Am. Chem. Soc.* **113**, 8426–8437 (1991).
13. Paine, R. T. & Nöth, H. Recent advances in phosphinoborane chemistry. *Chem. Rev.* **95**, 343–379 (1995).
14. Knabel, K., Klapötke, T. M., Nöth, H., Paine, R. T. & Schwab, I. A bicyclic P–P-bridged 1,3,2,4-diphosphadiboretane cation and an imino(phosphinidene)borane–$AlBr_3$ adduct. *Eur. J. Inorg. Chem.* **2005**, 1099–1108 (2005).
15. Bailey, J. A. & Pringle, P. G. Monomeric phosphinoboranes. *Coord. Chem. Rev.* **297-298**, 77–90 (2015).
16. Price, A. N. & Cowley, M. J. Base-stabilized phosphinidene boranes by silylium-ion abstraction. *Chem. Eur. J.* **22**, 6248–6252 (2016).
17. Price, A. N., Nichol, G. S. & Cowley, M. J. Phosphaborenes: accessible reagents for the synthesis of C–C/P–B isosteres. *Angew. Chem. Int. Ed.* **56**, 9953–9957 (2017).
18. Yang, W. et al. Crystalline BP-doped phenanthryne via photolysis of the elusive boraphosphaketene. *Angew. Chem. Int. Ed.* **59**, 3971–3975 (2020).
19. Koner, A., Morgenstern, B. & Andrada, D. M. Metathesis reactions of a NHC-stabilized phosphaborene. *Angew. Chem. Int. Ed.* **61**, e202203345 (2022).
20. Li, J., Lu, Z. & Liu, L. L. A free phosphaborene stable at room temperature. *J. Am. Chem. Soc.* **144**, 23691–23697 (2022).
21. Li, J., Mei, Y. & Liu, L. L. An isolable phosphaborene stabilized by an intramolecular Lewis base. *Eur. J. Inorg. Chem.* **2022**, e202200368 (2022).
22. LaPierre, E. A., Patrick, B. O. & Manners, I. A Crystalline Monomeric Phosphaborene. *J. Am. Chem. Soc.* **145**, 7107–7112 (2023).
23. Rivard, E., Merrill, W. A., Fettinger, J. C. & Power, P. P. A donor-stabilization strategy for the preparation of compounds featuring P=B and As=B double bonds. *Chem. Commun.* **2006**, 3800–3802 (2006).
24. Rivard, E. et al. Boron–pnictogen multiple bonds: donor-stabilized P=B and As=B bonds and a hindered iminoborane with a B–N triple bond. *Inorg. Chem.* **46**, 2971–2978 (2007).
25. Hardman, N. J., Cui, C., Roesky, H. W., Fink, W. H. & Power, P. P. Stable, monomeric imides of aluminum and gallium: synthesis and characterization of $[\{HC(MeCDippN)_2\}MN\text{-}2,6\text{-}Trip_2C_6H_3]$ (M=Al or Ga; Dipp=2,6-*i*$Pr_2C_6H_3$; Trip=2,4,6-*i*$Pr_3C_6H_2$). *Angew. Chem. Int. Ed.* **40**, 2172–2174 (2001).
26. Li, J. et al. Synthesis, structure, and reactivity of a monomeric iminoalane. *Chem. Eur. J.* **18**, 15263–15266 (2012).
27. Anker, M. D., Schwamm, R. J. & Coles, M. P. Synthesis and reactivity of a terminal aluminium–imide bond. *Chem. Commun.* **56**, 2288–2291 (2020).
28. Heilmann, A., Hicks, J., Vasko, P., Goicoechea, J. M. & Aldridge, S. Carbon monoxide activation by a molecular aluminium imide: C–O bond cleavage and C–C bond formation. *Angew. Chem. Int. Ed.* **59**, 4897–4901 (2020).
29. Dhara, D. et al. Synthesis and reactivity of a dialane-bridged diradical. *Angew. Chem, Int. Ed.* **63**, e202401052 (2024).
30. Feng, G. & Yamashita, M. Synthesis and reactivity of an alumanyl–tin species to form an Al,N-heteroallene derivative. *J. Am. Chem. Soc.* **146**, 28653–28657 (2024).
31. Queen, J. D., Irvankoski, S., Fettinger, J. C., Tuononen, H. M. & Power, P. P. A monomeric aluminum imide (Iminoalane) with Al–N triple-bonding: bonding analysis and dispersion energy stabilization. *J. Am. Chem. Soc.* **143**, 6351–6356 (2021).
32. Wright, R. J., Phillips, A. D., Allen, T. L., Fink, W. H. & Power, P. P. Synthesis and characterization of the monomeric imides Ar'MNAr" (M = Ga or In; Ar' or Ar" = terphenyl ligands) with two-coordinate gallium and indium. *J. Am. Chem. Soc.* **125**, 1694–1695 (2003).
33. Wright, R. J., Brynda, M., Fettinger, J. C., Betzer, A. R. & Power, P. P. Quasi-isomeric gallium amides and imides $GaNR_2$ and RGaNR (R = Organic Group): reactions of the digallene, Ar'GaGaAr' (Ar' = C_6H_3-2,6-(C_6H_3-2,6-Pr^i_2)$_2$) with unsaturated nitrogen compounds. *J. Am. Chem. Soc.* **128**, 12498–12509 (2006).
34. Anker, M. D., Lein, M. & Coles, M. P. Reduction of organic azides by indyl-anions. isolation and reactivity studies of indium–nitrogen multiple bonds. *Chem. Sci.* **10**, 1212–1218 (2019).
35. von Hänisch, C. & Hampe, O. $\{Li(thf)_3\}_2Ga_2\{As(SiiPr_3)\}_4$—A compound with gallium-arsenic double bonds. *Angew. Chem. Int. Ed.* **41**, 2095–2097 (2002).
36. Ganesamoorthy, C. et al. From stable Sb- and Bi-centered radicals to a compound with a Ga=Sb double bond. *Nat. Commun.* **9**, 87 (2018).
37. Helling, C., Wölper, C. & Schulz, S. Synthesis of a gallaarsene $\{HC[C(Me)N\text{-}2,6\text{-}i\text{-}Pr_2\text{-}C_6H_3]_2\}GaAsCp^*$ containing a Ga=As double bond. *J. Am. Chem. Soc.* **140**, 5053–5056 (2018).

38. García-Romero, Á, Hu, C., Pink, M. & Goicoechea, J. M. A crystalline unsupported phosphagallene and phosphaindene. *J. Am. Chem. Soc.* **147**, 1231–1239 (2025).
39. Wilson, D. W. N., Feld, J. & Goicoechea, J. M. A phosphanyl-phosphagallene that functions as a frustrated Lewis pair. *Angew. Chem. Int. Ed.* **59**, 20914–20918 (2020).
40. Li, B., Wölper, C., Haberhauer, G. & Schulz, S. Synthesis and reactivity of heteroleptic Ga–P–C allyl cation analogues. *Angew. Chem. Int. Ed.* **60**, 1986–1991 (2021).
41. Sharma, M. K., Wölper, C., Haberhauer, G. & Schulz, S. Multitalented gallaphosphene for Ga–P–Ga heteroallyl cation generation, CO_2 storage, and C(sp^3)–H bond activation. *Angew. Chem. Int. Ed.* **60**, 6784–6790 (2021).
42. Sharma, M. K. et al. $(PCO)_2$ (M = Ga, In): a new class of reactive group 13 metal-phosphorus compounds. *Chem. Eur. J.* **28**, e202200444 (2022).
43. Feld, J., Wilson, D. W. N. & Goicoechea, J. M. Contrasting E–H bond activation pathways of a phosphanyl-phosphagallene. *Angew. Chem. Int. Ed.* **60**, 22057–22061 (2021).
44. Szych, L. S., Bresien, J., Fischer, L., Ernst, M. J. & Goicoechea, J. M. Reactivity of an arsanyl-phosphagallene: decarbonylation of CO_2 and COS to form phosphaketenes. *Chem. Sci.* **16**, 7397–7410 (2025).
45. Wilson, D. W. N., Myers, W. K. & Goicoechea, J. M. Synthesis and decarbonylation chemistry of gallium phosphaketenes. *Dalton Trans* **49**, 15249–15255 (2020).
46. Taeufer, T. et al. Photochemical formation and reversible base-induced cleavage of a phosphagallene. *Chem. Sci.* **14**, 3018–3023 (2023).
47. Wang, Y. et al. Synthesis and reactivity of germyl-substituted gallapnictenes. *Inorg. Chem.* **64**, 3485–3494 (2025).
48. Nees, S. et al. On the reactivity of Mes*P(PMe_3) towards aluminum(I) compounds – evidence for the intermediate formation of phosphaalumenes. *ChemPlusChem* **88**, e202300078 (2023).
49. Szych, L. S., Denker, L., Feld, J. & Goicoechea, J. M. Trapping an elusive phosphanyl-phosphaalumene. *Chem. Eur. J.* **30**, e202401326 (2024).
50. Fischer, M. et al. Isolable phospha- and arsaalumenes. *J. Am. Chem. Soc.* **143**, 4106–4111 (2021).
51. Nees, S. et al. On the reactivity of phosphaalumenes towards C–C multiple bonds. *Angew. Chem. Int. Ed.* **62**, e202215838 (2023).
52. Wellnitz, T. et al. Reactivity of pnictaalumenes towards 1,3-dipole molecules. *Angew. Chem. Int. Ed.* **64**, e202506356 (2025).
53. Wellnitz, T., Wu, L., Braunschweig, H. & Hering-Junghans, C. A BNAlP-heterocycle. *Chem. Commun.* **61**, 4014–4017 (2025).
54. Luo, Q., Liu, T., Huang, L., Yang, C. & Lu, W. Aromative dephosphinidenation of a bisphosphirane-fused anthracene toward E–H (E=H, Si, N and P) bond activation. *Angew. Chem. Int. Ed.* **63**, e202405122 (2024).
55. Luo, Q., Liu, T., Huang, L., Li, Q. & Lu, W. On the reactivity of bisphosphirane-fused anthracene towards dichalcogenide bonds, IPr carbene, 2,6-diisopropylphenyl isocyanide and trimethylsilyl azide. *Eur. J. Org. Chem.* **28**, e202500071 (2025).
56. Lu, T. & Chen, F. Multiwfn: a multifunctional wavefunction analyzer. *J. Comput. Chem.* **33**, 580–592 (2012).
57. Savin, A., Nesper, R., Wengert, S. & Fässler, T. F. ELF: the electron localization function. *Angew. Chem. Int. Ed. Engl.* **36**, 1808–1832 (1997).
58. Welch, G. C., Juan, R. R. S., Masuda, J. D. & Stephan, D. W. Reversible, metal-free hydrogen activation. *Science* **314**, 1124–1126 (2006).
59. Stephan, D. W. The broadening reach of frustrated Lewis pair chemistry. *Science* **354**, aaf7229 (2016).
60. Geier, S. J., Gilbert, T. M. & Stephan, D. W. Activation of H_2 by phosphinoboranes $R_2PB(C_6F_5)_2$. *J. Am. Chem. Soc.* **130**, 12632–12633 (2008).
61. Fan, J. et al. Silylene-stabilized neutral dibora-aromatics with a B=B bond. *J. Am. Chem. Soc.* **146**, 20458–20467 (2024).
62. Lu, W. et al. An unsymmetrical, cyclic diborene based on a chelating CAAC ligand and its small-molecule activation and rearrangement chemistry. *Angew. Chem. Int. Ed.* **61**, e202113947 (2022).
63. Lu, W., Xu, K., Li, Y., Hirao, H. & Kinjo, R. Facile activation of homoatomic σ bonds in white phosphorus and diborane by a diboraallene. *Angew. Chem. Int. Ed.* **57**, 15691–15695 (2018).
64. Xu, H. et al. Dialumene-mediated production of phosphines through P_4 reduction. *Angew. Chem. Int. Ed.* **63**, e202404532 (2024).
65. Holzner, R. et al. Imino(silyl)disilenes: application in versatile bond activation, reversible oxidation and thermal isomerization. *Dalton Trans* **50**, 8785–8793 (2021).
66. Fanta, A. D. et al. The reaction of disilenes with P_4 and As_4. *Inorg. Chim. Acta.* **198-200**, 733–739 (1992).
67. Driess, M., Fanta, A. D., Powell, D. R. & West, R. Synthesis, characterization, and complexation of an unusual P_2Si_2 bicyclobutane with butterfly-structure: 2,2,4,4-tetramesityl-1,3-diphospha-2,4-disilabicyclo[1.1.0]butane. *Angew. Chem. Int. Ed. Engl.* **28**, 1038–1040 (1989).
68. Fox, A. R., Wright, R. J., Rivard, E. & Power, P. P. $Tl_2[Aryl_2P_4]$: a thallium complexed diaryltetraphosphabutadienediide and its two-electron oxidation to a diaryltetraphosphabicyclobutane, $Aryl_2P_4$. *Angew. Chem. Int. Ed. Engl.* **44**, 7729–7733 (2005).
69. Khan, S. et al. Preparation of RSn(I)–Sn(I)R with two unsymmetrically coordinated Sn(I) atoms and subsequent gentle activation of P_4. *J. Am. Chem. Soc.* **133**, 17889–17894 (2011).
70. Drieß, M. 1,2,3-triphospha-4-silabicyclo[1.1.0]butanes from activated, stable phosphasilenes and white phosphorus. *Angew. Chem. Int. Ed. Engl.* **30**, 1022–1024 (1991).
71. Li, X., Cheng, X., Song, H. & Cui, C. Synthesis of $HC[(CBut)(NAr)]_2Al$ (Ar = 2,6-$Pri_2C_6H_3$) and its reaction with isocyanides, a bulky azide, and H_2O. *Organometallics* **26**, 1039–1043 (2007).
72. Chen, W. et al. Reductive linear- and cyclo-trimerization of isocyanides using an Al–Al-bonded compound. *Chem. Commun.* **55**, 9452–9455 (2019).
73. Evans, M. J., Anker, M. D., McMullin, C. L. & Coles, M. P. Controlled reductive C–C coupling of isocyanides promoted by an aluminyl anion. *Chem. Sci.* **14**, 6278–6288 (2023).
74. Coles, M. P. & Hitchcock, P. B. Variable coordination chemistry of the phospha(iii)guanidinate anion; application as a metal-functionalised phosphine ligand. *Chem. Commun.* **23**, 2794–2795 (2002).
75. Schmidpeter, A., Jochem, G., Karaghiosofl, K. & Robl, C. Phosphorus(v) selenides with phosphorus in a trigonal-planar environment. *Angew. Chem. Int. Ed. Engl.* **31**, 1350–1352 (1992).double bond is not shown clearly in the phenyl ring

Acknowledgements

This work was supported by the National Natural Science Foundation of China (22471177), the Sichuan Science and Technology Program (2024NSFSC0285, 2022ZYD0050), the Funding for Hundred Talent Program of Sichuan University (YJ2021161), and the Fundamental Research Funds for the Central Universities. We would like to thank Dr. Yongxin Li (NTU) and Meng Yang (Sichuan University) for support in Single-crystal X-ray diffraction analysis. We acknowledge Dongyan Deng and Jing Li at Sichuan University, and Qianli Li at Liaocheng University for assistance in NMR and HRMS measurement. We thank Dr. William C. Ewing (VanDeMark) for his kind support on the preparation of the manuscript.

Author contributions

Y.C., X.Z. F.L. X.N., T.L., and Q.L. carried out the experiment work. Z.Y. and P.G. conducted theoretical studies. W.L. conceived and supervised the study. Y.C., Z.Y., and W.L. drafted the manuscript. All authors contributed to discussions.

Competing interests

The authors declare no competing interests.

Additional information

Supplementary information The online version contains supplementary material available at https://doi.org/10.1038/s41467-026-69118-4.

Correspondence and requests for materials should be addressed to Wei Lu.

Peer review information *Nature Communications* thanks the anonymous reviewer(s) for their contribution to the peer review of this work. A peer review file is available.